Third-order numerical schemes for hyperbolic problems

Jean-Antoine Desideri, Aurélien Goudjo, Vittorio Selmin

▶ **To cite this version:**

Jean-Antoine Desideri, Aurélien Goudjo, Vittorio Selmin. Third-order numerical schemes for hyperbolic problems. [Research Report] RR-0607, INRIA. 1987. inria-00075947

HAL Id: inria-00075947
https://inria.hal.science/inria-00075947

Submitted on 24 May 2006

HAL is a multi-disciplinary open access archive for the deposit and dissemination of scientific research documents, whether they are published or not. The documents may come from teaching and research institutions in France or abroad, or from public or private research centers.

L'archive ouverte pluridisciplinaire **HAL**, est destinée au dépôt et à la diffusion de documents scientifiques de niveau recherche, publiés ou non, émanant des établissements d'enseignement et de recherche français ou étrangers, des laboratoires publics ou privés.

INRIA

CENTRE
SOPHIA ANTIPOLIS

Institut National
de Recherche
en Informatique
et en Automatique

Domaine de Voluceau
Rocquencourt
B.P.105
78153 Le Chesnay Cedex
France
Tél. (1) 39 63 55 11

Rapports de Recherche

N° 607

THIRD-ORDER NUMERICAL SCHEMES FOR HYPERBOLIC PROBLEMS

Jean-Antoine DESIDERI
Aurélien GOUDJO
Vittorio SELMIN

Février 1987

THIRD-ORDER NUMERICAL SCHEMES FOR HYPERBOLIC PROBLEMS

SCHEMAS NUMERIQUES DU TROISIEME ORDRE
POUR LA RESOLUTION DE PROBLEMES HYPERBOLIQUES

Jean-Antoine DESIDERI
Aurélien GOUDJO
Vittorio SELMIN

INRIA Sophia-Antipolis
Avenue Émile Hugues
(Anc. Route des Lucioles)
Sophia Antipolis
06565 VALBONNE

ABSTRACT

Explicit third-order accurate schemes applicable to a one-dimensional linear test-equation are first constructed. Among these are considered an extension of the "Hancock-van Leer" upwind predictor/corrector scheme, and a scheme based on the "method of lines" in which the time-integration is performed by a Runge-Kutta method of order 3. Both of these approaches have been used recently by other authors for more ambitious calculations [1-3]. A comparison between these schemes is made by a detailed analysis of the dissipation error and the phase error in terms of a parameter controlling the degree of upwinding introduced in the spatial approximation.

Extensions to several dimensions are then examined from a theoretical standpoint (Fourier Analysis-Modified Equation) and by numerical experiments conducted (a) on linear problems with variable coefficients ("Rotating Concentration-Cone), and (b) in a nonlinear hyperbolic context (Supersonic Euler Flows).

In general, we conclude that the method of lines seems to offer the simplest and most efficient alternative to construct a third-order accurate scheme in a multidimensional nonlinear hyperbolic context.

RESUME

On utilise d'abord une équation test linéaire monodimensionnelle pour construire des schémas explicites précis au troisième ordre. On considère notamment une extension du schéma prédicteur/correcteur décentré de "Hancock-van Leer" ainsi qu'un schéma de type "méthode des lignes" utilisant un intégrateur en temps de Runge-Kutta d'ordre 3. Ces deux types de schéma ont été récemment utilisés par d'autres auteurs pour des calculs plus ambitieux [1-3]. Une analyse comparative de ces schémas est faite en examinant dans le détail l'erreur de dissipation et l'erreur de phase en fonction d'un paramètre qui contrôle le degré de décentrage de l'approximation spatiale.

Des extensions au cas multidimensionnel sont ensuite examinées d'un point de vue théorique (Analyse de Fourier-Equation Equivalente) et par des expériences numériques portant sur des problèmes (a) linéaires à coefficients variables ("Problème de la tâche tournante"), et (b) nonlinéaires (Equations d'Euler en régime supersonique).

La conclusion générale est que la méthode des lignes semble fournir l'alternative la plus simple et la plus efficace pour construire un schéma précis au troisième ordre dans un contexte hyperbolique nonlinéaire multidimensionnel.

PAPIER RÉCUPÉRÉ ET RECYCLÉ

Contents

I. INTRODUCTION

For classical aeronautical applications (supersonic flow simulations), a variety of second-order accurate methods are today available and efficiently utilized to solve a wide class of problems. However, for solving more complex flows, such as those encountered in the flight of a hypersonic vehicle, interest has recently gained for robust methods, possibly based on upwind differencing, but also for more accurate time-dependent solvers. In a similar context, Warming et al. [4] proposed a 3-step method in which an artificial viscosity term had to be adjusted to meet a certain stability criterion.

This report investigates some aspects of the construction and analysis of third-order accurate numerical schemes applicable to complex hyperbolic problems.

In Chapter II, schemes applicable to a typical one-dimensional hyperbolic equation are constructed and studied in details.

In Chapter III, extensions to two dimensions are considered. In particular, computations of nonlinear problems governed by the Euler Equations are made.

II. THIRD-ORDER SCHEMES IN ONE SPACE DIMENSION

In this Chapter, third-order schemes applicable to the one-dimensional convection equation

$$u_t + cu_x = 0 \quad (c > 0) \tag{1}$$

are constructed, analyzed and compared by numerical experiments.

1. Construction

In this Section, we first recall a technique due to Fromm [5] to construct a third-order scheme from two second-order schemes whose phase errors are of opposite signs. We then extend this technique to the construction of two other schemes by optimally adjusting a parameter β controlling the degree of upwinding. Ultimately, we alternately consider a more classical third-order scheme based on the method of lines.

1.1. *Fromm Method (FR)*

We consider two well-known second-order approximation schemes to the wave equation:

the Lax-Wendroff method [7] (LW):

$$u_j^{n+1} = u_j^n - \frac{c\Delta t}{2\Delta x}(u_{j+1}^n - u_{j-1}^n) + \frac{c^2(\Delta t)^2}{2(\Delta x)^2}(u_{j+1}^n - 2u_j^n + u_{j-1}^n) \tag{2}$$

the upwind method [7] (UW):

$$u_j^{n+1} = u_j^n - \frac{c\Delta t}{2\Delta x}(3u_j^n - 4u_{j-1}^n + u_{j-2}^n) + \frac{c^2(\Delta t)^2}{2(\Delta x)^2}(u_j^n - 2u_{j-1}^n + u_{j-2}^n) \tag{3}$$

Both schemes are based on a Taylor's series expansion of $u(t+\Delta t)$ that includes the second-order term and in which the derivatives are replaced by appropriate finite-differences. In the Lax-Wendroff method central differences are used, while in the upwind method backward differences instead.

These methods have known modified equations [7]:

LW:

$$u_t + cu_x = -c\frac{(\Delta x)^2}{6}(1-\nu^2)u_{xxx} - c\frac{(\Delta x)^3}{8}\nu(1-\nu^2)u_{xxxx} + \cdots \tag{4}$$

UW:

$$u_t + cu_x = +c\frac{(\Delta x)^2}{6}(1-\nu)(2-\nu)u_{xxx} - c\frac{(\Delta x)^3}{8}\nu(1-\nu)^2(2-\nu)u_{xxxx} + \cdots \tag{5}$$

In these equations ν is the Courant number:

$$\nu = \frac{c\Delta t}{\Delta x} \tag{6}$$

The LW method is stable for $\nu \leq 1$, while the UW method is stable for $\nu \leq 2$ [7]. Note that these conditions both correspond to the positivity of the coefficient of $-u_{xxxx}$ which is the lowest-order dissipation term in the equation. This condition is always a necessary condition of stability (stability of the low-frequency modes); here, it is also sufficient.

It is apparent that both schemes are second-order accurate. Consequently, the principal part of the error is proportional to the the third derivative u_{xxx}; it is a *phase* error. In addition, for $\nu \leq 1$, the coefficients corresponding to both schemes are of opposite signs. Thus, for such Courant numbers, the LW scheme has a predominently *lagging* phase error, while UW scheme has a predominently *leading* phase error. This observation naturally leads one to attempt to eliminate the principal part of the phase error by appropriately linearly combining the two schemes. More precisely, one considers the following approximation scheme:

$$(1-\beta)(\text{LW}) + \beta(\text{UW}) \tag{7}$$

in which β is adjustable ($0 \leq \beta \leq 1$), and defined as the "upwinding parameter" since it serves to weight the central-differencing scheme, LW ($\beta = 0$) and the fully-upwind scheme, UW ($\beta = 1$). Expliciting the difference-equation associated with this scheme gives:

$$\begin{aligned} u_j^{n+1} = u_j^n &- \frac{c\Delta t}{2\Delta x}\left((1-\beta)(u_{j+1}^n - u_{j-1}^n) + \beta(3u_j^n - 4u_{j-1}^n + u_{j-2}^n)\right) \\ &+ \frac{c^2(\Delta t)^2}{2(\Delta x)^2}\left((1-\beta)(u_{j+1}^n - 2u_j^n + u_{j-1}^n) + \beta(u_j^n - 2u_{j-1}^n + u_{j-2}^n)\right) \end{aligned} \tag{8}$$

Now if the condition $(1-\beta)(\nu^2-1)+\beta(1-\nu)(2-\nu)=0$ is enforced, that is

$$\beta = \frac{\nu+1}{3} \tag{9}$$

the second-order term in the truncation error is eliminated. The modified equation associated with the corresponding scheme is:

$$u_t + cu_x = -c\frac{(\Delta x)^3}{24}(2-\nu)(1-\nu^2)u_{xxxx} + \cdots \tag{10}$$

This scheme is due to Fromm [5]. It is clearly third-order accurate.

The stability and efficiency of Fromm's scheme will be evaluated in Sections 2 and 3. Prior to this, we observe that if this construction successfully yields a third-order accurate scheme, the method requires the evaluation of two second-order schemes and its implementation in a multidimensional case may reveal costly. For this reason, alternatively, other schemes will be constructed in the following Subsections that also rely on an adjustable upwinding, this time introduced in a more economical way.

1.2. *A Predictor/Corrector Method (PC)*

A second-order accurate scheme in both time and space can be achieved by a predictor/corrector sequence provided the space differences employed in the corrector step are at least second-order accurate. One possibility is to apply a centered predictor step, which is economical to evaluate, followed by a corrector step in which central and (2nd-order) backward differences are combined for a variable upwinding, that is:s

Predictor:

$$\tilde{u}_j = u_j^n - \frac{c\Delta t}{4\Delta x}(u_{j+1}^n - u_{j-1}^n) \tag{11}$$

Corrector:

$$u_j^{n+1} = u_j^n - \frac{c\Delta t}{2\Delta x}\left((1-\beta)(\tilde{u}_{j+1}-\tilde{u}_{j-1}) + \beta(3\tilde{u}_j - 4\tilde{u}_{j-1} + \tilde{u}_{j-2})\right) \tag{12}$$

Computing the modified equation of this scheme yields:

$$u_t + cu_x = -c\frac{(\Delta x)^2}{6}(1-\nu^2-3\beta)u_{xxx} - c\frac{(\Delta x)^3}{8}\left(2\beta(1-\nu)-\nu^3\right)u_{xxxx} + \cdots \tag{13}$$

Several observations can be made from this equation: (1) for any β the scheme is at least second-order accurate; (2) the principal parts of the phase errors corresponding to $\beta = 0$ (central scheme) and $\beta = 1$ (fully upwind scheme) are of opposite signs; (3) again, for an intermediate value of β, namely,

$$\beta = \frac{1 - \nu^2}{3} \tag{14}$$

third-order accuracy is achieved; (4) finally, for $\beta = 0$, the coefficient of u_{xxxx} in the truncation error is positive, regardless the value of the Courant number ν. This implies the instability of the low-frequency modes. This is no surprise since the scheme then solely combines explicit Euler steps based on central differences. Although the precise stability limit of this scheme will be evaluated in Section 2, it can yet be anticipated that even for a larger value of β ($\beta > 0$), the scheme is too severely restricted by stability to be efficient, despite the progress realized by the predictor/corrector formulation. For this reason, we now turn to a more ingenious construction of a predictor/corrector scheme.

1.3. *A Generalization of the Hancock-van Leer Scheme (HVL)*

The Hancock-van Leer scheme [8] is made to apply more generally to a conservation law, say

$$u_t + \big(f(u)\big)_x = 0 \tag{15}$$

where the "flux" $f(u)$ is some (nonlinear) function of u whose Jacobian, $A(u) = \frac{\partial f}{\partial u}$, in the case of a system ($u, f \in R^m$, $m > 1$), has real eigenvalues (hyperbolicity). It is formulated as follows:

Predictor (centered and linearized):

$$\tilde{u}_j = u_j^n - \frac{\Delta t}{2} A(u_j) u'_j \tag{16}$$

where $u'_j = \frac{u_{j+1}^n - u_{j-1}^n}{2\Delta x}$ is referred to as a "slope".

Corrector:
(a) interpolation of predicted values to cell boundaries:

$$\begin{aligned} \tilde{u}_{(j-\frac{1}{2})^+} &= \tilde{u}_j - \frac{\Delta x}{2} u'_j \\ \tilde{u}_{(j+\frac{1}{2})^-} &= \tilde{u}_j + \frac{\Delta x}{2} u'_j \end{aligned} \tag{17}$$

(b) update (second-order, conservative):

$$u_j^{n+1} = u_j^n - \frac{\Delta t}{\Delta x}(\Phi_{j+\frac{1}{2}} - \Phi_{j-\frac{1}{2}}) \tag{18}$$

where, for all i,

$$\Phi_{i+\frac{1}{2}} = \Phi\left(\tilde{u}_{(i+\frac{1}{2})^-}, \tilde{u}_{(i+\frac{1}{2})^+}\right) \tag{19}$$

in which $\Phi(u,v)$ is an appropriate numerical flux-function consistent with the flux $f(u)$ in the sense that

$$\Phi(u,u) = f(u) \tag{20}$$

for any u in the domain of f. One possible choice for Φ is given by []:

$$\Phi(u,v) = \frac{f(u)+f(v)}{2} + \frac{1}{2}\left|A\left(\frac{u+v}{2}\right)\right|(u-v) \tag{21}$$

This scheme is the result of a judicious construction:
(a) The form given to the integration step in the corrector is such that it realizes a conservative upwind scheme thus capable of correctly capturing weak solutions.
(b) The predictor/corrector formulation produces a second-order time-integration method easy to implement.
(c) The interpolation of cell-boundary-values results in a second-order accurate scheme in space.
(d) Computational efficiency is achieved by the vectorizable linearization of the predictor (in multidimensional applications), and the use of the same slopes $\{u'_j\}$ in the interpolations as in the predictor step.

These are some of the reasons why the "HVL" scheme is a very attractive explicit second-order upwind scheme. We now return to the simpler context of the wave equation, with $c > 0$, where the expression of the numerical flux trivially reduces to:

$$\begin{aligned}\Phi(u,v) &= \frac{cu+cv}{2} + \frac{1}{2}c(u-v) \\ &= cu \\ &= f(u)\end{aligned} \tag{22}$$

One simple way to introduce an adjustable degree of upwinding consists in only modifying the interpolation formula in the corrector steps and to leave all the integration steps unchanged. There, u'_j can be replaced by a linear combination of the forward and the backward differences of u, that is:

$$\bar{u}'_j = (1-\beta)\frac{u_{j+1}^n - u_j^n}{\Delta x} + \beta\frac{u_j^n - u_{j-1}^n}{\Delta x} \tag{23}$$

Thus for $\beta = \frac{1}{2}$, $\bar{u}'_j = u'_j$, and the original HVL scheme is obtained. Otherwise and in the case of the wave equation, the extended HVL scheme can be defined, in summary, by the following sequence:

Predictor:

$$\tilde{u}_j = u_j^n - \frac{c\Delta t}{4\Delta x}(u_{j+1}^n - u_{j-1}^n) \tag{24}$$

Corrector:
(a) interpolation:

$$\begin{aligned} \bar{u}'_j &= (1-\beta)\frac{u_{j+1}^n - u_j^n}{\Delta x} + \beta\frac{u_j^n - u_{j-1}^n}{\Delta x} \\ \tilde{u}_{(j+\frac{1}{2})^-} &= \tilde{u}_j + \frac{\Delta x}{2}\bar{u}'_j \\ \tilde{u}_{(j-\frac{1}{2})^+} &= \tilde{u}_j - \frac{\Delta x}{2}\bar{u}'_j \qquad \text{(unused if } c > 0) \end{aligned} \tag{25}$$

(b) integration:

$$u_j^{n+1} = u_j^n - \frac{c\Delta t}{\Delta x}(\tilde{u}_{(j+\frac{1}{2})^-} - \tilde{u}_{(j-\frac{1}{2})^-}) \tag{26}$$

We evaluated the modified equation of this scheme and found:

$$\begin{aligned} u_t + cu_x = &-c\frac{(\Delta x)^2}{6}(1 + \frac{3}{2}\nu - \nu^2 - 3\beta)u_{xxx} \\ &-c\frac{(\Delta x)^3}{8}\left(2\beta(1-2\nu) + 2\nu^2 - \nu^3\right)u_{xxxx} + \cdots \end{aligned} \tag{27}$$

We can observe that regardless the value of β, the method is (at least) second-order accurate in both time and space. It thus respects the judicious construction by Hancock-van Leer. Moreover, letting

$$\beta = \frac{1 + \frac{3}{2}\nu - \nu^2}{3} \tag{28}$$

third-order accuracy is achieved.

In conclusion, a third-order accurate explicit predictor/corrector scheme has been constructed. Note that here the result is attained more economically since the adjustment of the upwinding only affects the interpolation step and leaves the more costly integration steps unchanged.

Finally, for the sake of completeness, we consider in the next subsection the construction of a fourth third-order scheme, this last one based on the method of lines.

1.4. *Method of Lines (RK3)*

In the method of lines, the unknown is defined as the vector $U = \{u_j\}$ whose components are approximations to the grid-values of u. One first selects an approximation to the spatial derivative , here cu_x. For example:

$$\Psi_j(U) = (1-\beta)\left(c\frac{u_{j+1}-u_{j-1}}{2\Delta x}\right) + \beta\left(c\frac{3u_j - 4u_{j-1}+u_{j-2}}{2\Delta x}\right) \tag{29}$$

where again β is an adjustable coefficient.
Substituting this in the p.d.e. yields a set of ordinary differential equations:

$$U_t + \Psi(U) = 0 \tag{30}$$

which can be solved by a Runge-Kutta method. Since the aim of this study is to construct third-order schemes, the Runge-Kutta 3 method (RK3) is employed:

$$\begin{cases} U^{(0)} = U^n \\ U^{(1)} = U^{(0)} - \dfrac{\Delta t}{3}\Psi(U^{(0)}) \\ U^{(2)} = U^{(0)} - \dfrac{\Delta t}{2}\Psi(U^{(1)}) \\ U^{(3)} = U^{(0)} - \dfrac{\Delta t}{1}\Psi(U^{(2)}) \\ U^{n+1} = U^{(3)} \end{cases} \tag{31}$$

Strictly speaking, this method is third-order accurate for linear o.d.e.'s only, whereas another formulation of the RK3 method exists that is third-order accurate in the nonlinear case also; but the latter requires more computer storage and is more complex to implement and is not considered here for these reasons.

In order to evaluate the modified equation of this integration scheme, we introduce the characteristic polynomial of RK3:

$$g(z) = 1 + z + \frac{z^2}{2} + \frac{z^3}{6} \tag{32}$$

The value of this polynomial is equal to the amplification factor of the RK3 method when it is applied to the linear test equation:

$$U_t = \lambda U \tag{33}$$

Then:

$$U^{n+1} = g(z)U^n \tag{34}$$

where $z = \lambda\Delta t$. [1] In the case of a linear p.d.e.,say the wave equation, the above two equations are still valid if λ now stands for the "approximation matrix" defined as the matrix for which:

$$\Psi(U) = -\lambda U \tag{35}$$

Therefore we have:

$$\begin{aligned} \frac{U^{n+1} - U^n}{\Delta t} &= \frac{g(\lambda\Delta t) - 1}{\Delta t} U^n \\ &= \left(\lambda + \frac{\Delta t}{2}\lambda^2 + \frac{\Delta t^2}{6}\lambda^3\right) U^n \end{aligned} \tag{36}$$

We now switch to a functional notation. A Taylor's series expansion of $\Psi(u)$ gives:

$$\begin{aligned} \Psi(u) &= u_x + (1 - 3\beta)\frac{\Delta x^2}{6} u_{xxx} + \beta\frac{\Delta x^3}{4} u_{xxxx} + O(\Delta x^4) \\ &= -\lambda u \end{aligned} \tag{37}$$

yielding:

$$\lambda = -c\left(\frac{\partial}{\partial x} + (1 - 3\beta)\frac{\Delta x^2}{6}\frac{\partial^3}{\partial x^3} + \beta\frac{\Delta x^3}{4}\frac{\partial^4}{\partial x^4} + O(\Delta x^4)\right) \tag{38}$$

and consequently:

$$\begin{cases} \lambda^2 = c^2\left(\dfrac{\partial^2}{\partial x^2} + (1 - 3\beta)\dfrac{\Delta x^2}{3}\dfrac{\partial^4}{\partial x^4} + O(\Delta x^3)\right) \\ \lambda^3 = -c^3\left(\dfrac{\partial^3}{\partial x^3} + O(\Delta x^2)\right) \end{cases} \tag{39}$$

[1] Note that the exact solution $u_e(t)$ satisfies: $u_e((n+1)\Delta t) = e^z u_e(n\Delta t)$; hence the *local error* is proportional to the difference $g(z) - e^z$ and is of the order of $z^4 = O(\Delta t^4)$ which is characteristic of a third-order method.

Substituting these expressions into (36) and expanding the left-hand side in a time series give:

$$\begin{aligned} u_t + \frac{\Delta t}{2}u_{tt} + \frac{\Delta t^2}{6}u_{ttt} + \frac{\Delta t^3}{24}u_{tttt} + O(\Delta t^4) = \\ - c\left(u_x + (1-3\beta)\frac{\Delta x^2}{6}u_{xxx} + \beta\frac{\Delta x^3}{4}u_{xxxx} + O(\Delta x^4)\right) \\ + c^2\frac{\Delta t}{2}\left(u_{xx} + (1-3\beta)\frac{\Delta x^2}{3}u_{xxxx} + O(\Delta x^3)\right) \\ - c^3\frac{\Delta t^2}{6}\left(u_{xxx} + O(\Delta x^2)\right) \end{aligned} \tag{40}$$

From this point the classical technique for deriving modified equations can be applied. We found:

$$u_t + cu_x = c(3\beta - 1)\frac{\Delta x^2}{6}u_{xxx} - c\left(\beta\frac{\Delta x^3}{4} + \frac{c^3\Delta t^3}{24}\right)u_{xxxx} + \cdots \tag{41}$$

where only fourth-order terms have been omitted.

As expected, we observe that the method is in general second-order accurate and that it is for $\beta = \frac{1}{3}$ that it becomes third-order accurate.

In the next section we analyze the stability and efficiency of the various third-order methods constructed in this Section.

2. Stability and Efficiency

The stability of the various previously defined schemes was evaluated by Fourier analysis. For this, one injects in the finite-difference equation a single Fourier mode, say

$$u_j^n = Cg_\theta^n e^{i\theta} \tag{42}$$

where C is a constant, θ is a *frequency parameter* and g_θ is the unknown *amplification factor* corresponding to this particular mode. After some simplifications, we found the following expressions for g_θ:

FR:

$$g_\theta = 1 - \nu\left((1-\beta)i\sin\theta + \beta\frac{3 - 4e^{-i\theta} + e^{-2i\theta}}{2}\right) + \nu^2(\cos\theta - 1)\left(1 - \beta + \beta e^{-i\theta}\right) \tag{43}$$

PC:

$$g_\theta = 1 - \nu\left(1 - \frac{\nu}{2} i \sin\theta\right)\left((1-\beta) i \sin\theta + \beta \frac{3 - 4e^{-i\theta} + e^{-2i\theta}}{2}\right) \tag{44}$$

HVL:

$$g_\theta = 1 - \nu\left(1 - e^{-i\theta}\right)\left(1 - \frac{\nu}{2} i \sin\theta + \frac{1-\beta}{2}(e^{i\theta} - 1) + \frac{\beta}{2}(1 - e^{-i\theta})\right) \tag{45}$$

For RK3, the substitution of (42) in (29) gives:

$$\Psi_j^n = -\lambda_\theta u_j^n \tag{46}$$

where

$$-\lambda_\theta = \frac{c}{\Delta x}\left((1-\beta) i \sin\theta + \beta \frac{3 - 4e^{-i\theta} + e^{-2i\theta}}{2}\right) \tag{47}$$

Then,

$$g_\theta = g(z_\theta) \tag{48}$$

where $z_\theta \stackrel{\text{def}}{=} \lambda_\theta \Delta t$ is proportional to ν and the function g is defined by (32). Note that for all four cases,

$$g_{\pi-\theta} = \overline{g_\theta} \tag{49}$$

Consequently, when all possible Fourier modes are present in the solution, the amplification factor may be defined as:

$$\mathbf{g}(\nu) \stackrel{\text{def}}{=} \max_{\theta \in [0,\pi]} |g_\theta| \tag{50}$$

and the stability criterion reduces to:

$$\mathbf{g}(\nu) \leq 1 \tag{51}$$

In practice, for a given Courant number ν, the maximum was taken over a discrete set of values of θ. This allowed us to obtain the function $\mathbf{g}(\nu)$,and thus to determine the stability limit, $\nu_{\max}$. The plots of $\mathbf{g}(\nu)$ are given in Figure 1 and it follows that:

$$\nu_{\max} = \begin{cases} 1 & \text{for FR,} \\ 0.57 & \text{for PC,} \\ 1 & \text{for HVL,} \\ 1.62 & \text{for RK3.} \end{cases} \tag{52}$$

We conclude from these numbers that HVL and RK3 are the most efficient of these third-order schemes. In the next section these schemes are evaluated by numerical experiment.

3. Dissipation and Phase Error

For this hyperbolic (non-dissipative) model problem, the dissipative properties of a numerical scheme can be evaluated by comparing the modulus of the amplification factor $|g_\theta|$, with unity. The relative phase error is appreciated by forming the ratio $\frac{\Phi}{\Phi_e}$ in which Φ is the argument of the amplification factor, and analogously, $\Phi_e = Arg\big(u_e(x,t+\Delta t)/u_e(x,t)\big) = -\nu\theta$ ($u_e(x,t)$ = the exact solution). These parameters are plotted on Figures 2 and 3 for the different schemes as functions of the frequency parameter θ and for various values of the Courant number ν.

Comparing the plots of the relative phase error corresponding to the LW and UW schemes reveals that for a Courant number less than 1 and over more than 2/3 of the frequency-spectrum, the two schemes have opposed and practically symmetrical effects. As a result, weighting these schemes as realized by Fromm's scheme substantially reduces the phase error. In particular, this error is exactly anihilated at $\nu = \frac{1}{2}$.

In the case of the other third-order schemes, much like for Fromm's scheme, the phase error is importantly diminished by the optimal adjustment of the upwinding, in particular, and not surprisingly, at low frequencies. We note however that RK3 is the most dissipative scheme. Finally, we remark that in the case of a one-dimensional scalar equation the Fromm scheme and the HVL scheme are identical, as a simple calculation that we omit here would show.

4. Numerical Experiments and Conclusions

To illustrate the properties of the different schemes, the spatially periodic problem defined by (1) and the following initial condition, given over a period $0 \le x \le 1$ by

$$u_0(x) = \begin{cases} 1 & \text{if } |x - \frac{1}{2}| \le \frac{2}{10}, \\ 0 & \text{otherwise,} \end{cases} \tag{53}$$

was solved numerically. The exact solution of this problem is obtained by propagating at speed c the initial periodic profile. Thus the computation allows us to simulate the propagation of discontinuities in a linear context.

The solutions obtained by the application of the different numerical schemes with $\nu = \frac{1}{2}$ are plotted on Figure 4 at $t = 1/c$, that is after 1 time-period. The exact solution u_e is indicated on the figure, and also the value of the l2-norm of the

error,

$$E = \left(\frac{1}{N} \sum_{i=1}^{N} (u_j^n - u_e(j\Delta x, n\Delta t))^2 \right)^{\frac{1}{2}} \tag{54}$$

The experiments were carried out with 100 subdivisions/spacial period ($N = 100$).

When applying either second-order scheme (LW or UW), rather important oscillations appear near the discontinuities. These oscillations are noticeably diminished by the optimal adjustment of the upwinding which results in third-order accuracy. One can observe that the LW-scheme has a leading phase error and the UW-scheme a lagging phase error which confirms and illustrates the analysis of the previous section.

The solutions produced by the various third-order schemes are very analogous; however, as mentioned before, the phase error of the Fromm scheme or the HVL scheme is equal to zero for $\nu = \frac{1}{2}$, and this results in a perfect symmetry of the oscillations from both sides of the discontinuities.

In conclusion, since the accuracy of the different schemes was found very similar, in the following chapters where two-dimensional situations and nonlinear problems will be examined, only the HVL and RK3 methods will be considered since they are the most efficient from the stability and the facility of implementation standpoints.

III. TWO-DIMENSIONAL EXTENSIONS

1. The HVL Scheme in Two Dimensions

In this section, the convection equation extended to two space dimensions

$$u_t + au_x + bu_y = 0 \quad (a, b > 0) \tag{55}$$

is utilized as linear test-equation.

The HVL scheme again consists of a centered predictor followed by a corrector step in which firstly, interpolations are made to the cell-boundary-points before a conservative flux-splitting integration step is applied. Adjustable upwinding is again inserted in the interpolations, which introduces one parameter for each direction, β in x and γ in y. This gives:

Predictor:

$$\tilde{u}_{j,k} = u^n_{j,k} - \frac{\Delta t}{2}\left(a\frac{u^n_{j+1,k} - u^n_{j-1,k}}{2\Delta x} + b\frac{u^n_{j,k+1} - u^n_{j,k-1}}{2\Delta y}\right) \tag{56}$$

Corrector:
(a) interpolation:

$$\begin{aligned}
\bar{u}'_x)_{j,k} &= (1-\beta)\frac{u^n_{j+1,k} - u^n_{j,k}}{\Delta x} + \beta\frac{u^n_{j,k} - u^n_{j-1,k}}{\Delta x} \\
\tilde{u}_{(j+\frac{1}{2})^-,k} &= \tilde{u}_{j,k} + \frac{\Delta x}{2}\bar{u}'_x)_{j,k} \\
\tilde{u}_{(j-\frac{1}{2})^+,k} &= \tilde{u}_{j,k} - \frac{\Delta x}{2}\bar{u}'_x)_{j,k} \qquad \text{(unused if } a > 0\text{)} \\
\bar{u}'_y)_{j,k} &= (1-\gamma)\frac{u^n_{j,k+1} - u^n_{j,k}}{\Delta y} + \gamma\frac{u^n_{j,k} - u^n_{j,k-1}}{\Delta y} \\
\tilde{u}_{j,(k+\frac{1}{2})^-} &= \tilde{u}_{j,k} + \frac{\Delta y}{2}\bar{u}'_y)_{j,k} \\
\tilde{u}_{j,(k-\frac{1}{2})^+} &= \tilde{u}_{j,k} - \frac{\Delta y}{2}\bar{u}'_y)_{j,k} \qquad \text{(unused if } b > 0\text{)}
\end{aligned} \tag{57}$$

(b) integration:

$$u_{j,k}^{n+1} = u_{j,k}^{n} - \Delta t \left(a \frac{\tilde{u}_{(j+\frac{1}{2})^-,k} - \tilde{u}_{(j-\frac{1}{2})^-,k}}{\Delta x} + b \frac{\tilde{u}_{j,(k+\frac{1}{2})^-} - \tilde{u}_{j,(k-\frac{1}{2})^-}}{\Delta y} \right) \tag{58}$$

We evaluated the modified equation using brute-force Taylor's series. The calculation is straightforward but rather tedious. Only the result is presented here:

$$\begin{aligned} u_t + a u_x + b u_y = & P u_{xxx} + Q u_{xxy} + R u_{xyy} + S u_{yyy} \\ & + A_4 u_{xxxx} + A_3 u_{xxxy} + A_2 u_{xxyy} + A_1 u_{xyyy} + A_0 u_{yyyy} \\ & + \text{fourth} - \text{order terms} \end{aligned} \tag{59}$$

where:

$$\begin{cases} P = \dfrac{a^3}{6}\Delta t^2 - \dfrac{a^2}{4}\Delta t \Delta x + \dfrac{3\beta - 1}{6} a \Delta x^2 \\ Q = \dfrac{ab}{2}\Delta t (a\Delta t - \dfrac{\Delta x}{2}) \\ R = \dfrac{ab}{2}\Delta t (b\Delta t - \dfrac{\Delta y}{2}) \\ S = \dfrac{b^3}{6}\Delta t^2 - \dfrac{b^2}{4}\Delta t \Delta y + \dfrac{3\gamma - 1}{6} b \Delta y^2 \end{cases} \tag{60}$$

$$\begin{cases} A_4 = aP\Delta t - \dfrac{a\beta\Delta x^3}{4} + \dfrac{a^2 \Delta t \Delta x^2}{6} - \dfrac{a^3 \Delta t^3}{24} \\ A_3 = (aQ + bP)\Delta t + \dfrac{ab\Delta t \Delta x^2}{6} - \dfrac{a^3 b \Delta t^3}{6} \\ A_2 = (aR + bQ)\Delta t - \dfrac{a^2 b^2 \Delta t^3}{4} \\ A_1 = (aS + bR)\Delta t + \dfrac{ab\Delta t \Delta y^2}{6} - \dfrac{ab^3 \Delta t^3}{6} \\ A_0 = bS\Delta t - \dfrac{b\gamma \Delta y^3}{4} + \dfrac{b^2 \Delta t \Delta y^2}{6} - \dfrac{b^3 \Delta t^3}{24} \end{cases} \tag{61}$$

If one lets

$$\begin{cases} \nu = \dfrac{a\Delta t}{\Delta x} \\ \mu = \dfrac{b\Delta t}{\Delta y} \end{cases} \tag{62}$$

then P is annihilated by the same adjustment of the parameter of upwinding along the x-direction, that is for β satisfying (28). Similarly, S vanishes when γ is given by

the same formula with ν replaced by μ. However, this is not sufficient to eliminate all second-order terms, since the coefficients of the cross-derivatives, Q and R, are nonzero in general, unless the following condition is met

$$\nu = \mu = \frac{1}{2} \tag{63}$$

which requires that the mesh be such that

$$\frac{\Delta x}{a} = \frac{\Delta y}{b} \tag{64}$$

and that Δt be appropriately set. If these requirements can be satisfied for the linear constant-coefficient equation, they cannot however be met if the coefficients have an explicit dependence on x, y or t even in a linear context (p.d.e. linear in u). Hence, the direct two-dimensional extension of the HVL scheme cannot be made third-order accurate in the case of a p.d.e. with variable coefficients, $a = a(x,y,t)$, and/or $b = b(x,y,t)$.

An interesting remark can be made from (59-61). All second-order terms in Δt, Δx or Δy contribute to the dispersive error. Third-order terms contribute to the dissipation error. For a general eigenmode,

$$u(x) = Ce^{i(\omega_1 x + \omega_2 y)} \tag{65}$$

these terms sum up to $\tilde{\mu}(3)u(x)$ where:

$$\tilde{\mu}(3) = {\omega_1}^4 A_4 + {\omega_1}^3 \omega_2 A_3 + {\omega_1}^2 {\omega_2}^2 A_2 + \omega_1 {\omega_2}^3 A_1 + {\omega_2}^4 A_0 \tag{66}$$

Now suppose that Δx and Δy are held fixed, while Δt is left free but sufficiently small. Hence the behavior is determined by the values for $\Delta t = 0$. These are:

$$\begin{cases} P = \dfrac{3\beta - 1}{6} a \Delta x^2 \\ Q = R = 0 \\ S = \dfrac{3\gamma - 1}{6} b \Delta y^2 \end{cases} \tag{67}$$

$$\begin{cases} A_4 = -\dfrac{a\beta\Delta x^3}{4} \leq 0 \\ A_3 = A_2 = A_1 = 0 \\ A_0 = -\dfrac{b\gamma\Delta y^3}{4} \leq 0 \end{cases} \tag{68}$$

Also:

$$\begin{cases} \dfrac{\partial}{\partial \Delta t} A_4 = \dfrac{\beta a^2 \Delta x^2}{2} \leq 0 \\ \dfrac{\partial}{\partial \Delta t} A_3 = \dfrac{\beta ab \Delta x^2}{2} \leq 0 \\ \dfrac{\partial}{\partial \Delta t} A_2 = 0 \\ \dfrac{\partial}{\partial \Delta t} A_1 = \dfrac{\gamma ab \Delta y^2}{2} \leq 0 \\ \dfrac{\partial}{\partial \Delta t} A_0 = \dfrac{\gamma b^2 \Delta y^2}{2} \leq 0 \end{cases} \tag{69}$$

Consequently, for $\Delta t = 0$, A_4, A_3, A_2, A_1 and A_0 are negative and so is $\tilde{\mu}(3)$; as a result, the eigenmode is attenuated as t increases (dissipation). As Δt increases, the coefficients A_i's increase algebraically and so does $\tilde{\mu}(3)$ that first remains negative but diminishes in absolute value. Thus dissipation is reduced by increasing Δt.

2. Method of Lines (RK3)

The method of lines is extended to the multi-dimensional case in a straightforward fashion. Each derivative is differenced as in one dimension to form a flux function Ψ. For example, for the the 2-D convection equation, (55), abandoning here the assumption that $a, b > 0$, third-order accuracy is achieved with $\beta = \frac{1}{3}$ which gives:

$$\begin{aligned} \Psi_{j,k}(U) = \frac{1}{3}\left(a \frac{u_{j+1,k} - u_{j-1,k}}{2\Delta x} + b \frac{u_{j,k+1} - u_{j,k-1}}{2\Delta y} \right) \\ + \frac{2}{3}\left(a^+ \frac{3u_{j,k} - 4u_{j-1,k} + u_{j-2,k}}{2\Delta x} + a^- \frac{-3u_{j,k} + 4u_{j+1,k} - u_{j+2,k}}{2\Delta x} \right. \\ \left. + b^+ \frac{3u_{j,k} - 4u_{j,k-1} + u_{j,k-2}}{2\Delta y} + b^- \frac{-3u_{j,k} + 4u_{j,k+1} - u_{j,k+2}}{2\Delta y} \right) \end{aligned} \tag{70}$$

in which

$$\begin{cases} a^+ = \dfrac{a + |a|}{2} \\ a^- = \dfrac{a - |a|}{2} \end{cases} \quad \begin{cases} b^+ = \dfrac{b + |b|}{2} \\ b^- = \dfrac{b - |b|}{2} \end{cases} \tag{71}$$

so that

$$a = a^+ + a^-, \quad b = b^+ + b^- \tag{72}$$

with

$$a^+, b^+ \geq 0, \quad a^-, b^- \leq 0 \tag{73}$$

(If a and b were Jacobian matrices instead of being scalars, this would realize a "Flux-Splitting"; here, it simply selects the appropriate direction for upwinding).

Equation (29) being replaced by this definition, the equations of Section 1.4, from (30) to (36) are still applicable. In particular, in the linear case with constant coefficients or not, the method is third-order accurate in both time and space.

3. Dissipation and Phase Error

In two dimensions, a single eigenmode is defined by two frequency parameters ω_1 and ω_2, or equivalently by the following "wave-number vector":

$$\vec{\kappa} \stackrel{\text{def}}{=} (\omega_1 \Delta x, \omega_2 \Delta y) \tag{74}$$

The eigenvalue of the numerical scheme associated with this mode is denoted by $g_{\vec{\kappa},\vec{\nu}}$ since it also depends on the "Courant number vector"

$$\vec{\nu} \stackrel{\text{def}}{=} (\nu, \mu) \tag{75}$$

The (modulus of the) amplification factor is then expressed as follows:

$$\mathfrak{g}(\vec{\nu}) \stackrel{\text{def}}{=} \max_{\vec{\kappa} \in [0,\pi]^2} |g_{\vec{\kappa},\vec{\nu}}| \tag{76}$$

Consequently, in addition to the usual concept of dissipation error and phase error, appears in several dimensions, here two, a new type of error: numerical anisotropy which can be observed in the fact that in general $g_{\vec{\kappa},\vec{\nu}}$ is sensitive to the direction of the velocity vector (a,b), or equivalently to the vector $\vec{\nu}$.

To evaluate the properties of the various methods, we express the vector $\vec{\nu}$ as follows,

$$\vec{\nu} = \|\vec{\nu}\|(\cos\alpha, \sin\alpha) \tag{77}$$

in which α is the advection direction. To simplify the analysis, the response of the scheme is only examined in the case where the wave-numer vector is parallel to the advection direction, that is when:

$$\vec{\kappa} = \|\vec{\kappa}\|(\cos\alpha, \sin\alpha) \tag{78}$$

In the case of a square mesh, $\Delta x = \Delta y = h$, the wavelength λ is defined by:

$$\lambda \stackrel{\text{def}}{=} \frac{2\pi}{\|\overrightarrow{\omega}\|} = \frac{2\pi h}{\|\overrightarrow{\kappa}\|} \tag{79}$$

The properties of the HVL and RK3 schemes are compared on Figures 5 and 6 that provide a polar representation of the modulus of the amplification factor, $|g_{\overrightarrow{\kappa},\overrightarrow{\nu}}|$ and the relative phase error, $\frac{\Phi}{\Phi_e}$ ($\Phi_e = -(\nu\kappa_x + \mu\kappa_y)$), for several values of the parameter λ.

We observe that both schemes are more accurate for medium and long wavelengths and relatively more anisotropic for short wavelengths (high frequencies). For both schemes, the best accuracy is achieved when $\alpha = \frac{\pi}{4}$.

In general, it appears from the plots of the amplification factor and of the relative phase error, that preferrential directions exist in the propagation of the numerical solution. In particular, the stability limit is expressed differently in two dimensions, since it is given by a limit curve in the (ν, μ)-plane. This curve passes through the points $(\nu, \mu) = (\nu_{max}, 0)$ and $(0, \nu_{max})$ in which ν_{max} is given by (52) (one-dimensional limit), but also by the point $\nu = \mu = \nu'_{max}$ where

$$\nu'_{max} = \begin{cases} 0.68 & \text{for HVL,} \\ 1.22 & \text{for RK3.} \end{cases} \tag{80}$$

The condition

$$\|\overrightarrow{\nu}\| \leq \nu'_{max} \tag{81}$$

gives a sufficient stability condition.

Finally, we note that for RK3, when $\|\overrightarrow{\nu}\|$ increases, the dispersion error decreases, but the dissipation error increases.

4. Numerical Experiments on a Linear Variable-Coefficient Equation

As a first element of numerical comparison in two dimensions, we consider the following linear, variable-coefficient test problem:

$$\begin{cases} u_t + \overrightarrow{C}(x,y).\overrightarrow{gradu} = 0 & \text{over } \Omega =]-\frac{1}{2},\frac{1}{2}[\times]-\frac{1}{2},\frac{1}{2}[, \\ u(x,y,0) = u_0(x,y) & \text{over } \Omega, \\ u(x,y,t) = 0 & \text{along } \partial\Omega, \end{cases} \tag{82}$$

Here the convection speed is independent of u which results in a linear problem, but does depend explicitly on the cartesian coordinates x and y:

$$\vec{C} = (-y, x) \tag{83}$$

Two test problems will be examined that differ from the imposed initial solution u_0:

(a) Rotating Cosine-Hill:

$$\text{(P1)} \qquad u_0(x,y) = \begin{cases} \frac{1}{4}(1+\cos\pi\xi)(1+\cos\pi\eta) & \text{if } \xi^2+\eta^2 \le 1, \\ 0 & \text{otherwise,} \end{cases} \tag{84}$$

in which $\xi = (x-x_0)/\sigma$, $\eta = (y-y_0)/\sigma$ with $x_0 = y_0 = \frac{2}{10}$ and $\sigma = \frac{2}{10}$, and

(b) Rotating Concentration-Cone:

$$\text{(P2)} \qquad u_0(x,y) = \max_{x,y}\left(0, 1 - 5\sqrt{(x+\frac{1}{4})^2+y^2}\right) \tag{85}$$

In both cases, the exact solution of the problem at time t is obtained by rotating about the origin the initial solution of the angle $\theta = t$. In problem (P1) the initial solution is of class $C^1(\Omega)$, whereas in problem (P2) u_0 has discontinuous first derivatives along the boundary of its support.

The computations were performed using a 30×30 uniform mesh and $\Delta t = \frac{2\pi}{200}$. The numerical solutions corresponding to the initial solutions of (P1) and (P2) are indicated in Figures 7 and 8 at a time t corresponding to one revolution of the exact solution. To give a global idea of the accuracy, the maximum and the minimum values of the numerical solutions are indicated on the side of the plots together with the "average error",

$$E = \left(\frac{1}{N^2}\sum_{j,k=1}^{N}\left(u^n_{j,k} - u_e(j\Delta x, k\Delta y, n\Delta t)\right)^2\right)^{\frac{1}{2}} \tag{86}$$

The superior accuracy of the RK3 scheme is evident. The HVL scheme is overly dissipative, the dissipation acting primarily along streamlines. and being more important near the origin for a reason explained at the end of Section 1: in this region, the velocity and thus the Courant numbers are smaller , hence, Δt is effectively felt as "small".

Finally, we observe as expected, larger errors in the case of (P2) in which the exact solution is not smooth.

5. Computation of Two-Dimensional Euler Flows

To illustrate the behaviour of the numerical schemes in the nonlinear case, we solve the equations of gasdynamics for an inviscid, non-heat conducting fluid: the Euler equations. For completeness, we recall them here briefly. In conservative form, they are:

$$\frac{\partial U}{\partial t} + \frac{\partial F(U)}{\partial x} + \frac{\partial G(U)}{\partial y} = 0 \tag{87}$$

in which

$$U = \begin{pmatrix} \rho \\ m \\ n \\ e \end{pmatrix} \quad F = \begin{pmatrix} m \\ m^2/\rho + p \\ mn \\ (e+p)m/\rho \end{pmatrix} \quad G = \begin{pmatrix} n \\ mn \\ n^2/\rho + p \\ (e+p)n/\rho \end{pmatrix} \tag{88}$$

Here, U is the vector of conservative variables, F and G are the flux vectors in the x and y directions, $m = \rho u$ and $n = \rho v$ are the momentum components. The primitive variables are the density ρ, the velocity components u and v and the pressure p. For a polyatomic gas, the total energy per unit volume e is expressed in terms of these variables:

$$e = \frac{p}{\gamma - 1} + \frac{1}{2}\frac{m^2 + n^2}{\rho} \tag{89}$$

where γ is the ratio of specific heats ($\gamma = 1.4$ for air).

It is well known that the solutions of nonlinear problems by higher-order numerical schemes usually suffer from dispersive errors, visible by the presence of "ripples" in the plots of the unknowns, particularly near steep gradients. For this reason, to attempt to achieve the positivity of the scheme and to reduce the amplitude of the oscillations, flux-correctors or limiters were introduced [9,10].

First, the one-dimensional shock-tube problem used by Sod [11] to compare numerous popular numerical methods was solved. We chose a case in which an initial discontinuity breaks into a shock wave followed by a contact discontinuity and a rarefaction wave. The initial condition is given by:

$$\begin{cases} \rho = 1.0,\ m = 0.0,\ e = 2.5 & \text{for } 0 \le x \le \frac{1}{2} \\ \rho = 0.125,\ m = 0.0,\ e = 0.25 & \text{for } \frac{1}{2} \le x \le 1 \end{cases} \tag{90}$$

Calculations were made using a mesh of 101 points. The Courant number was set equal to 0.8. The numerical solution (pressure, velocity, mach number and density) is compared with the exact solution at time $t = 0.16$, on Figures 9 and 10 for the

HVL scheme and the RK3 method respectively. Note that since we are dealing with a vector equation and not a scalar one, it is not obvious which upwinding parameter β is optimum for the HVL scheme. We used successively $\beta = \frac{1}{2}$ and $\beta = \frac{1}{3}$. However, setting $\beta = \frac{1}{3}$ the RK3 method is third-order accurate.

We can observe that the HVL correctly captures the different singularities present in the solution. Also, by letting $\beta = \frac{1}{3}$ a more accurate solution is obtained, but the interaction of the choice of this parameter with the limiters is not yet known.

Slightly sharper discontinuities are obtained by the RK3 method. The solution is essentially monotonous with $\beta = \frac{1}{2}$ and very small oscillations appear with $\beta = \frac{1}{3}$, but the shock is perhaps steeper.

Both methods provide fairly accurate solutions to the shock-tube problem.

The second test problem is two-dimensional. It corresponds to the simulation of the interaction of an incident shock wave with a fixed obstacle as in [12-13] here a very simplified space shuttle profile. A finite-element formulation was used with a discretisation of the domain shown on Figure 11. The mesh is fixed in time and contains less than 1200 points. It is therefore very coarse. Letting the subscripts 1 and 2 correspond to the regions before and after the discontinuity, the initial condition is defined by:

$$\begin{cases} \rho_1 = 3.333 \\ m_1 = 2.3381 \\ n_1 = 0.0 \\ e_1 = 2.8523 \\ M_1 = 1.197 \end{cases} \quad \begin{cases} \rho_2 = 1.0 \\ m_2 = 0.0 \\ n_2 = 0.0 \\ e_2 = 0.2857 \\ M_2 = 0.0 \end{cases} \tag{91}$$

where $M = \sqrt{u^2 + v^2}/\sqrt{\frac{\gamma p}{\rho}}$ is the Mach number. These conditions represent a discontinuity that propagates at a speed equal to 1.

The calculation is made using the RK3 method. The resulting Mach contour lines are shown on Figure 12 at different times. We can observe the effects of the propagation of shock along the body. In particular three shocks can be distinguished: a detached shock ahead of the round nose, a shock emanating from the cabin and the incident shock. Once the incident shock is at the rear of the "vehicle" complex unsteady phenomena occur that the present method cannot evaluate because in particular to the inadequacy of the mesh employed here.

Nevertheless, we conclude in general that the method is sufficiently accurate to capture some of the interesting physical features of the flow.

IV. CONCLUSION

In this report we have constructed various schemes applicable to the solution of hyperbolic equations and conducted a theoretical systematic and comparative study of these schemes. In particular, by optimally adjusting the degree of upwinding in the spatial approximation, we were able in certain cases to achieve third-order accuracy.

In general, we conclude that the method of lines seems to provide the simplest and most efficient alternative to construct a third-order accurate method in a nontrivial situation.

V. REFERENCES

[1] ANDERSON, W. K., THOMAS, J. L., and van LEER, B. (1985), A Comparison of Finite-Volume Flux-Vector Splittings for the Euler Equations, AIAA Paper 85-0122.

[2] TURKEL, E., and van LEER, B. (1984), Flux-Vector Splitting and Runge-Kutta Methods for the Euler Equations, ICASE Report No. 84-27.

[3] RIZZI, A. (1982), Damped Euler-Equation Method to Compute Transonic Flow Around Wing-Body Combinations, AIAA J., vol. 20, No. 10. pp. 1321-1328.

[4] WARMING, R. F., KUTLER, P., and LOMAX, H. (1973), Second- and Third-Order Noncentered Difference Schemes for Nonlinear Hyperbolic Equations, AIAA J., vol. 11, pp.189-196.

[5] FROMM, J. E. (1968), A Method for Reducing Dispersion in Convective Difference Schemes, J. Comp. Phys., vol. 3, pp. 176-189.

[6] LASCAUX, P. (1976), Lectures on "Numerical Methods for Time-Dependent Equations - Applications to Fluid Flow Problems" Tata Institute of Fundamental Research, Bombay.

[7] ANDERSON, D. A., TANNEHILL, J. C., and PLETCHER, R. H. (1984), Computational Fluid Mechanics and Heat Transfer, Hemisphere Publishing Corporation, McGraw-Hill Book Company.

[8] van LEER, B. (1983), Computational Methods for Ideal Compressible Flow, von Karman Institute for Fluid Dynamics, Lecture Series 1983-04.

[9] DERVIEUX, A. (1985), Steady Euler Simulations Using Unstructured Meshe Von Karman Institute for Fluid Dynamics, Lecture Series 1985-04.

[10] FEZOUI, F. (1985), Résolution des Equations d'Euler par un Schéma de van Leer en Eléments Finis, Rapport de Recherche INRIA, Janvier 1985.

[11] SOD, G. A. (1978), A Survey of Several Finite-Difference Methods for Systems of Nonlinear Hyperbolic Conservation Laws, J. Comp. Phys.,

[12] MARK, A., KUTLER, P. (1983), Computation of Shock-Wave/Target Interaction, AIAA Paper 83-0039.

[13] YEE, H., and KUTLER, P. (1983), Application of Second-Order Accurate Total-Variation-Diminishing (TVD) Schemes to the Euler Equations in General Geometries, NASA TM 85845.

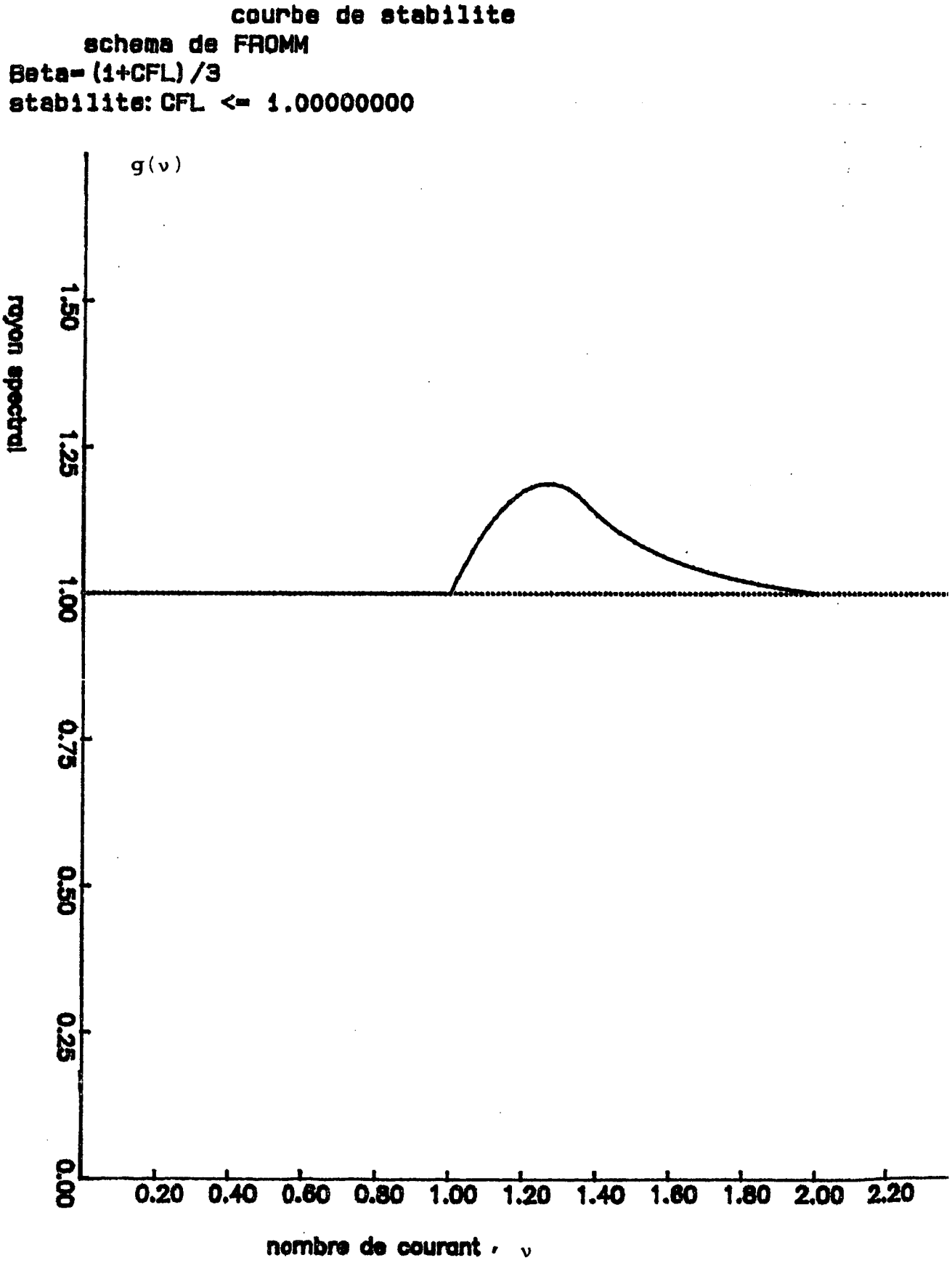

Figure 1. Amplification Factor (a) Fromm's scheme

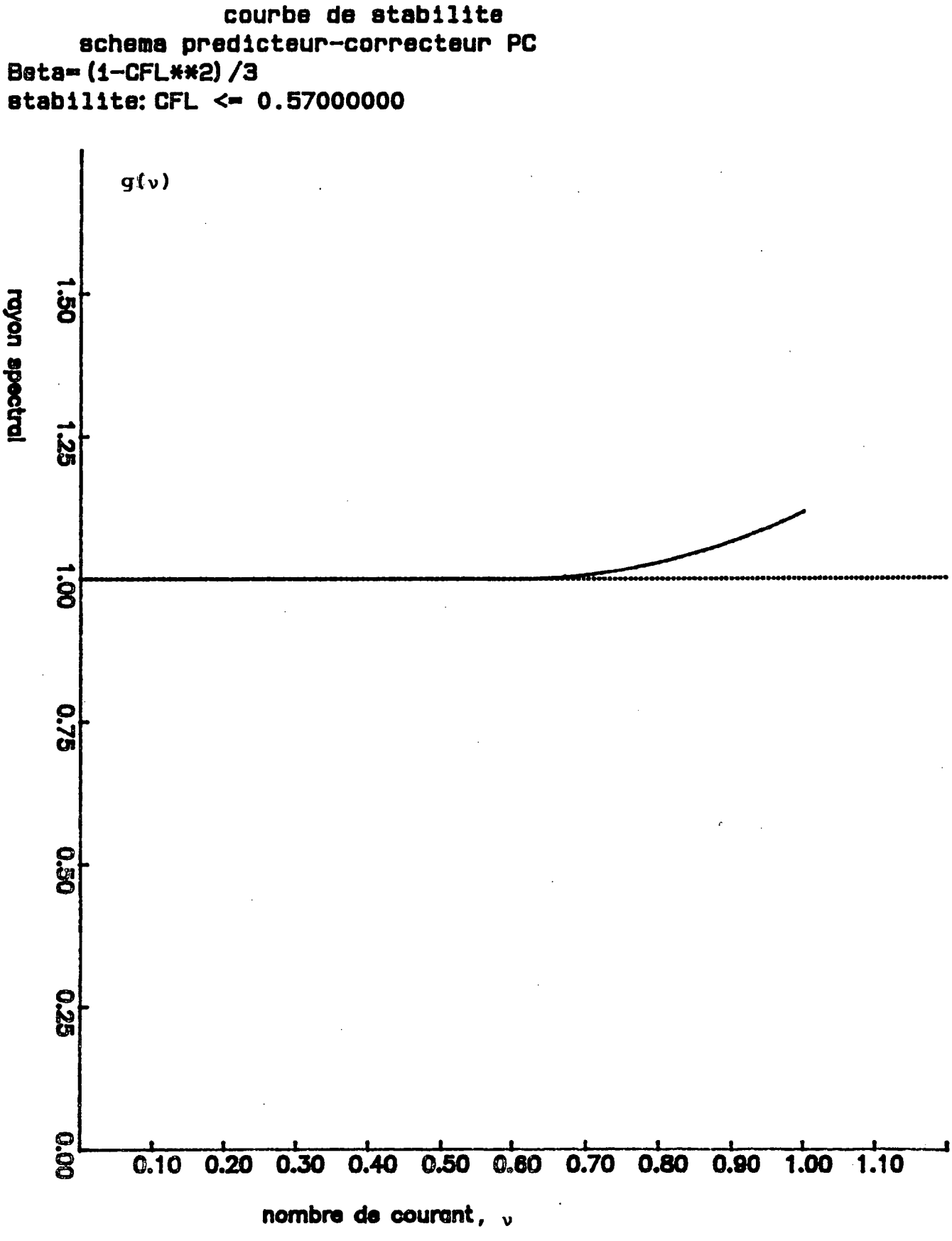

Figure 1. Cont'd (b) Predictor-Corrector scheme

courbe de stabilite
beta-schema Hancock/Van Leer
Beta optimal
stabilite: CFL <= 1.00000000

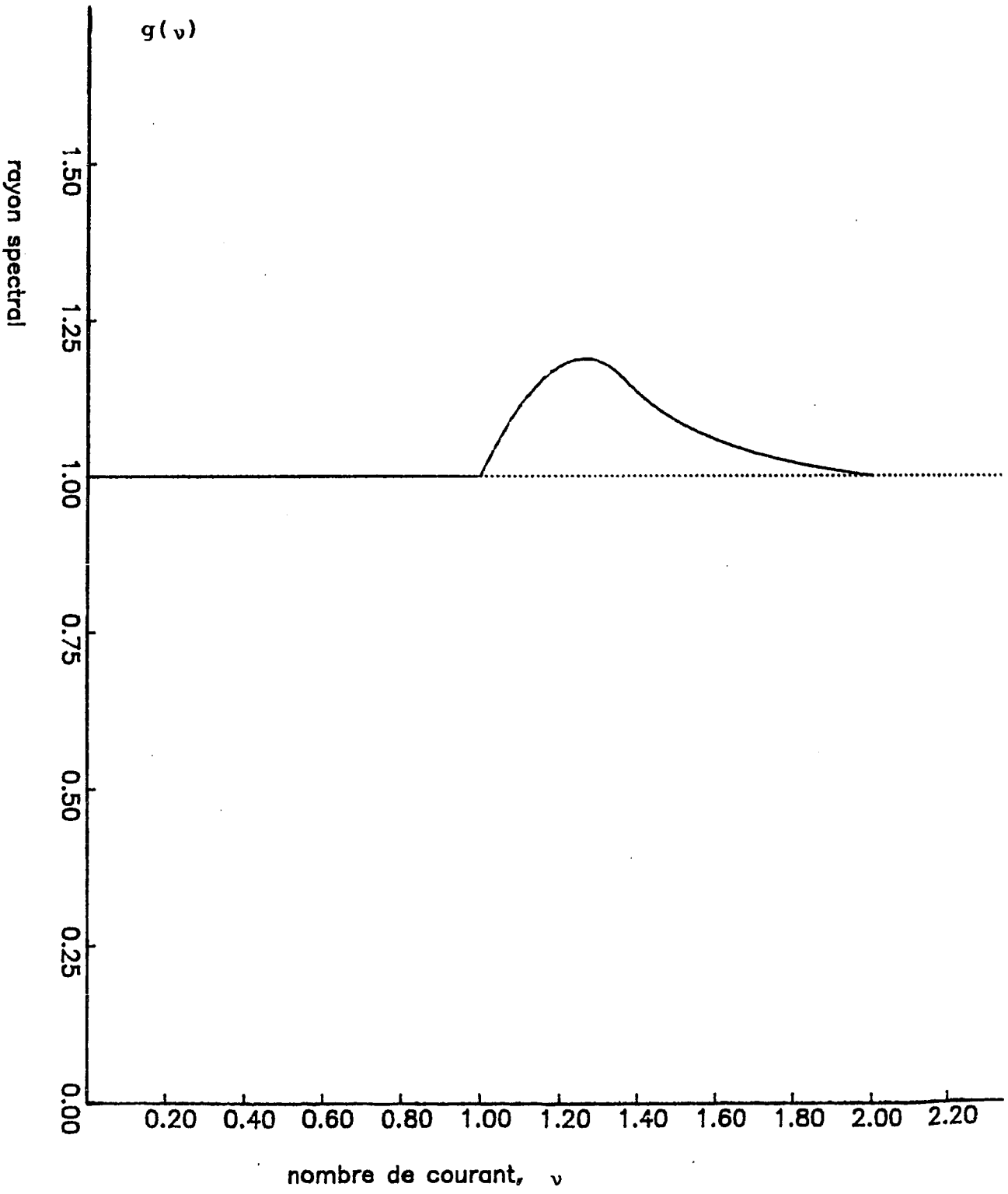

Figure 1. Cont'd (c) HVL scheme

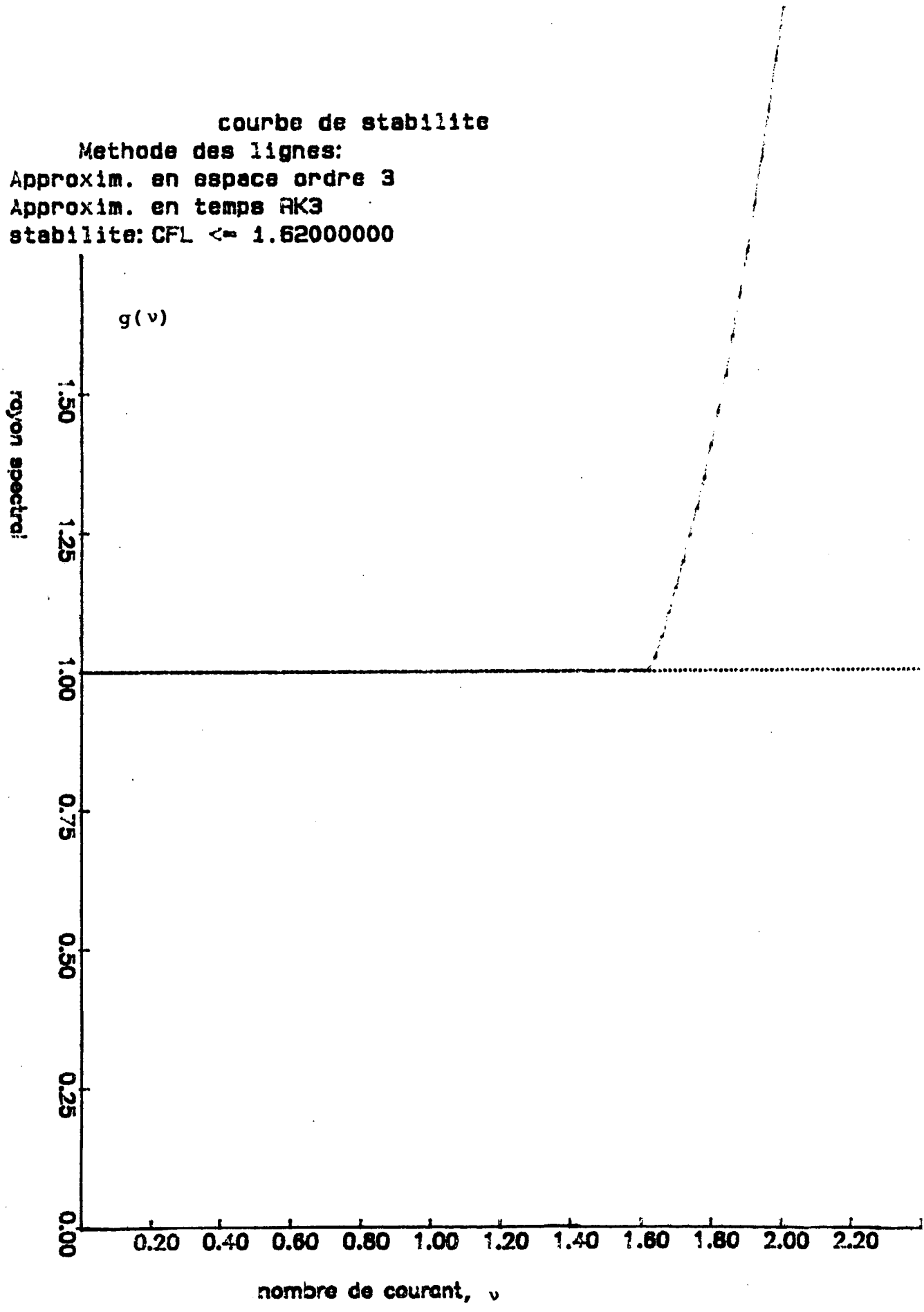

Figure 1. Concluded (d) RK3

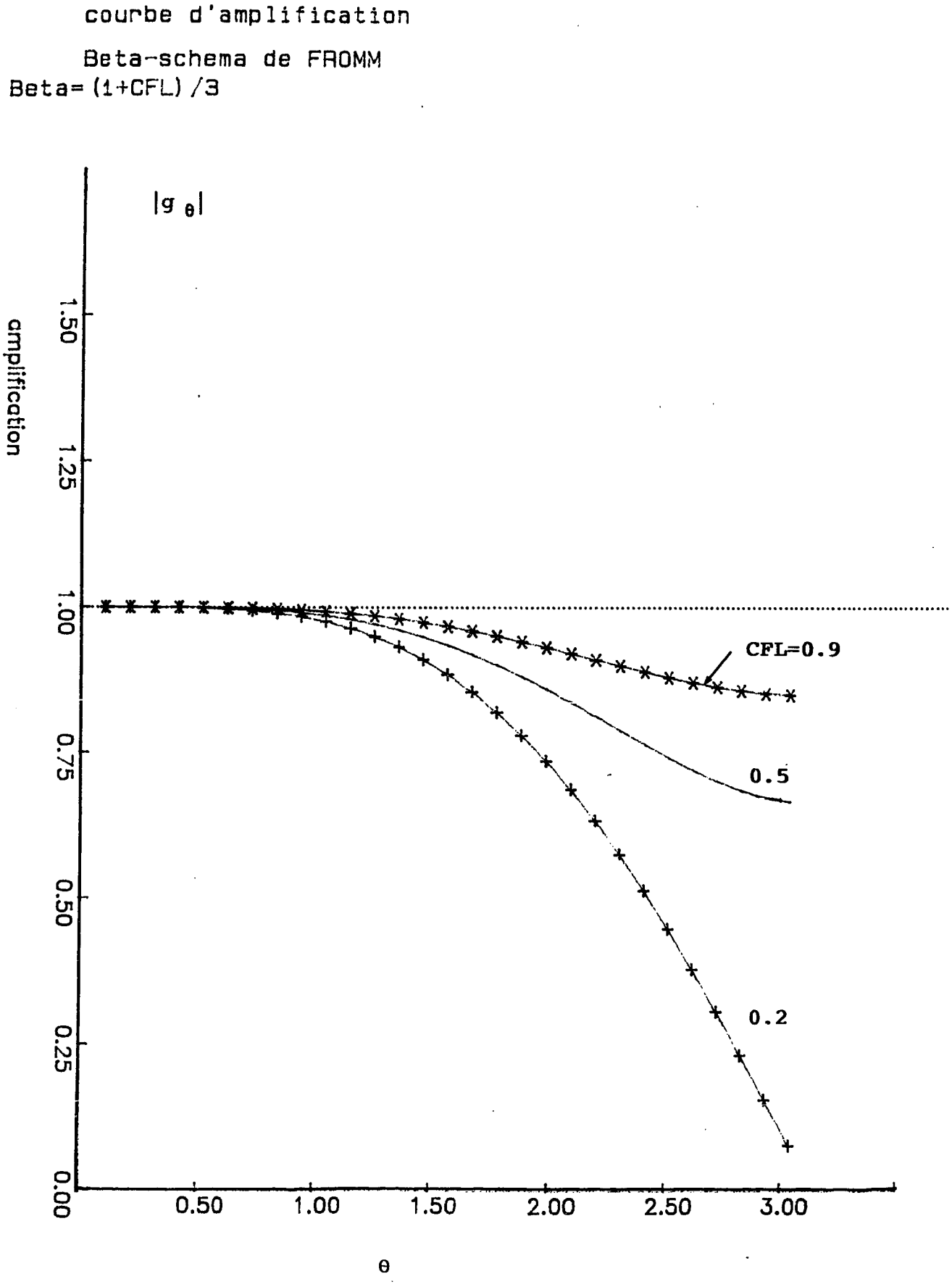

Figure 2. Dissipation Error (a) Fromm's scheme

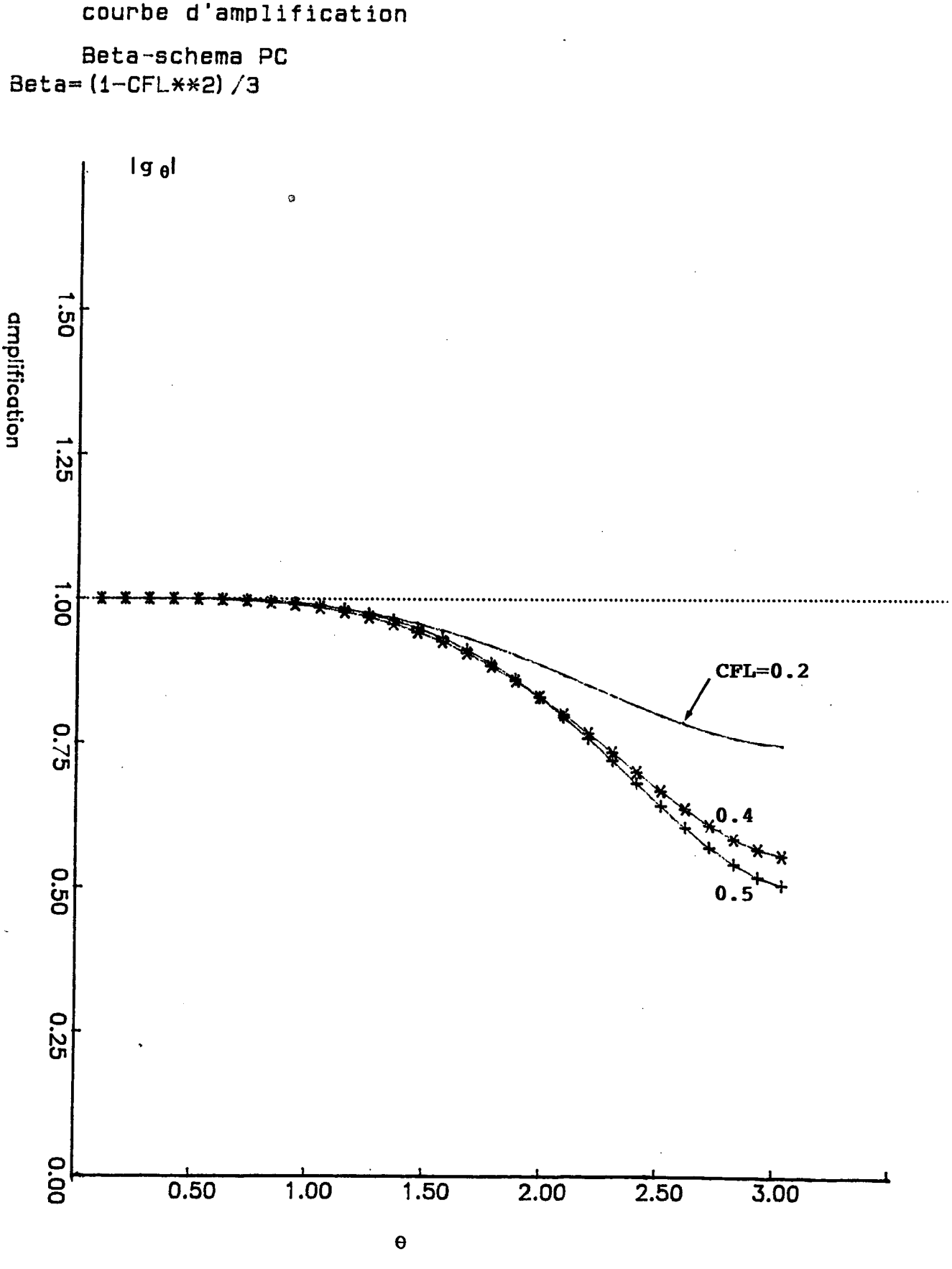

Figure 2. Cont'd (b) Predictor-Corrector scheme

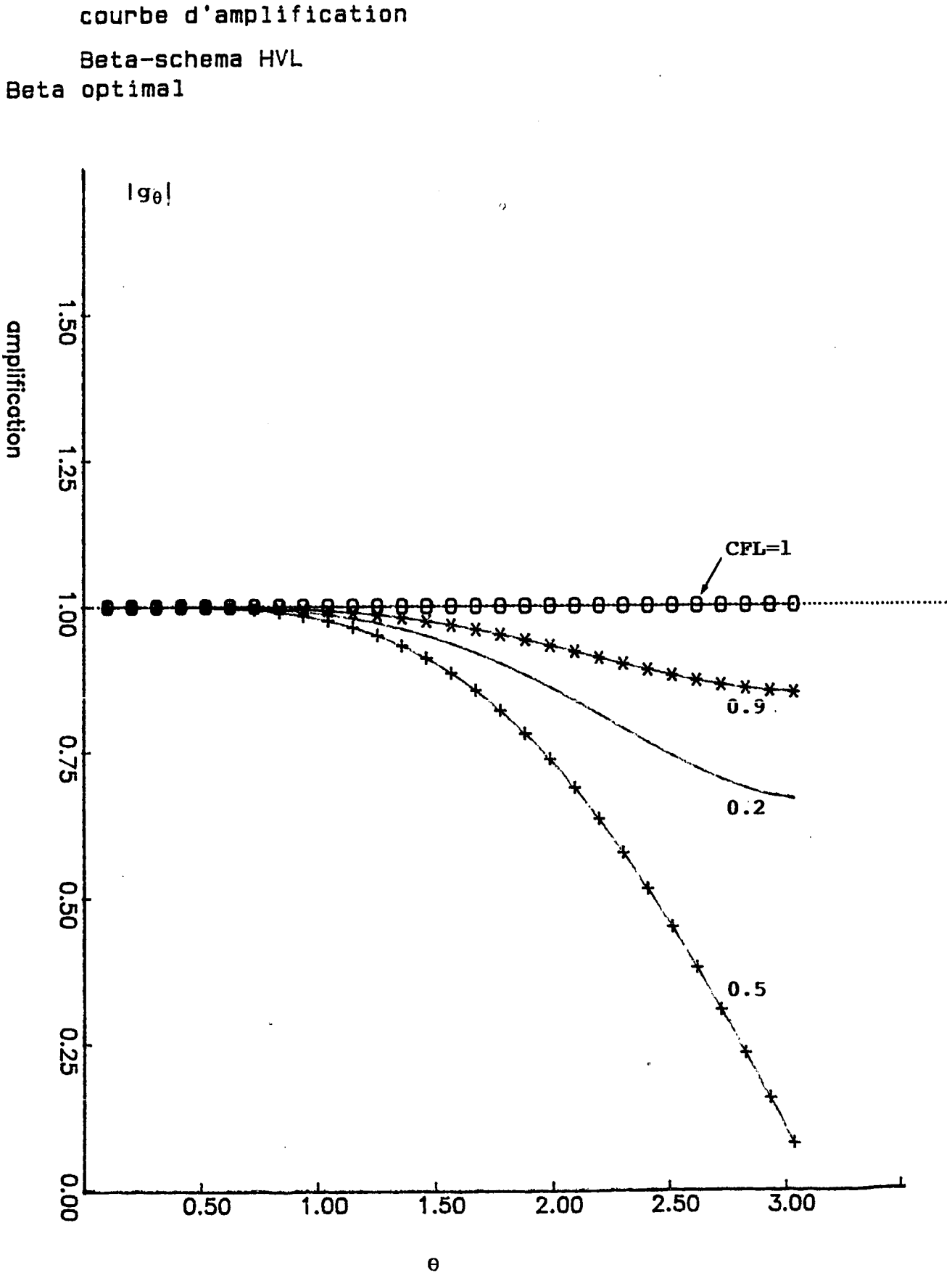

Figure 2. Cont'd (c) HVL scheme

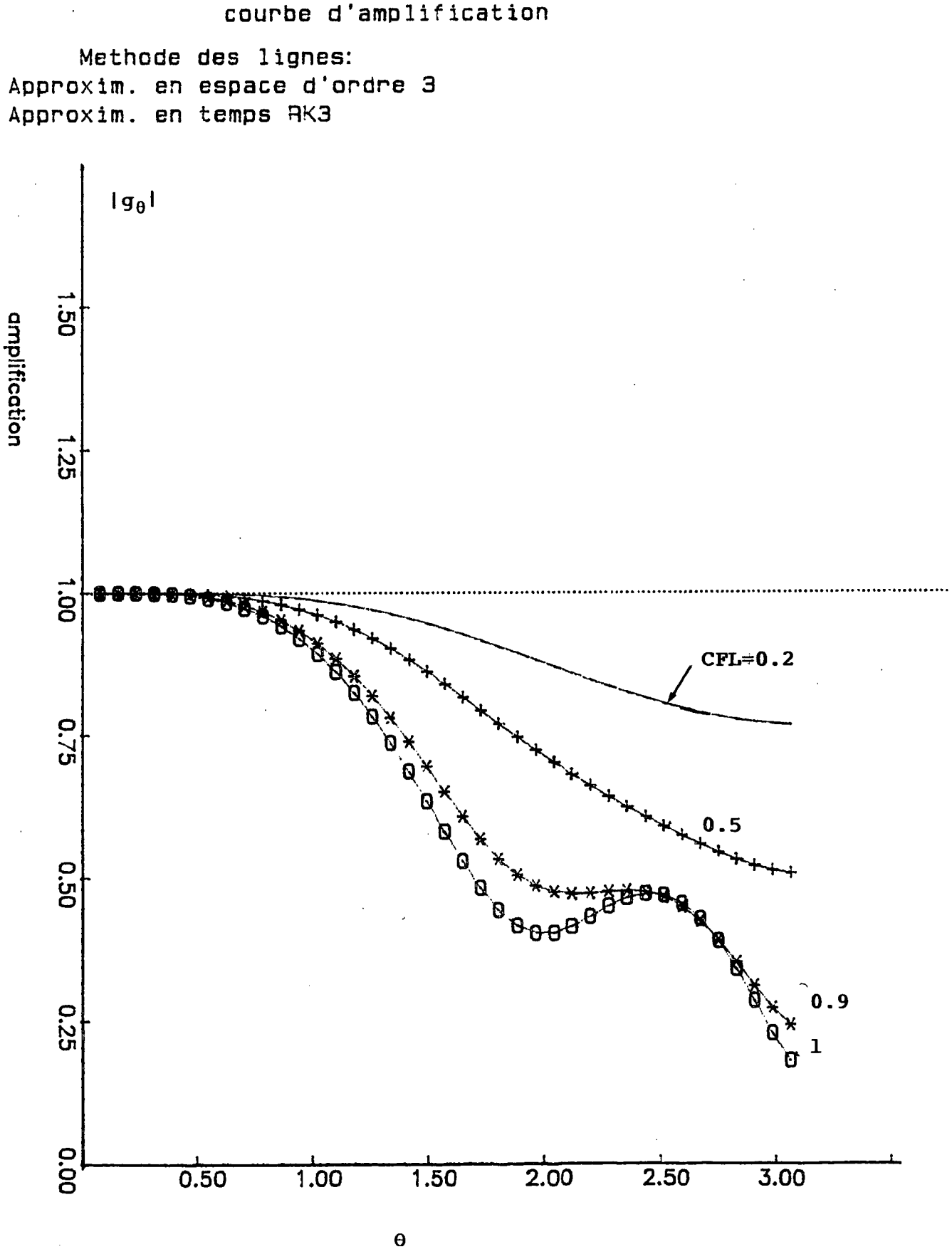

Figure 2. Concluded (d) RK3

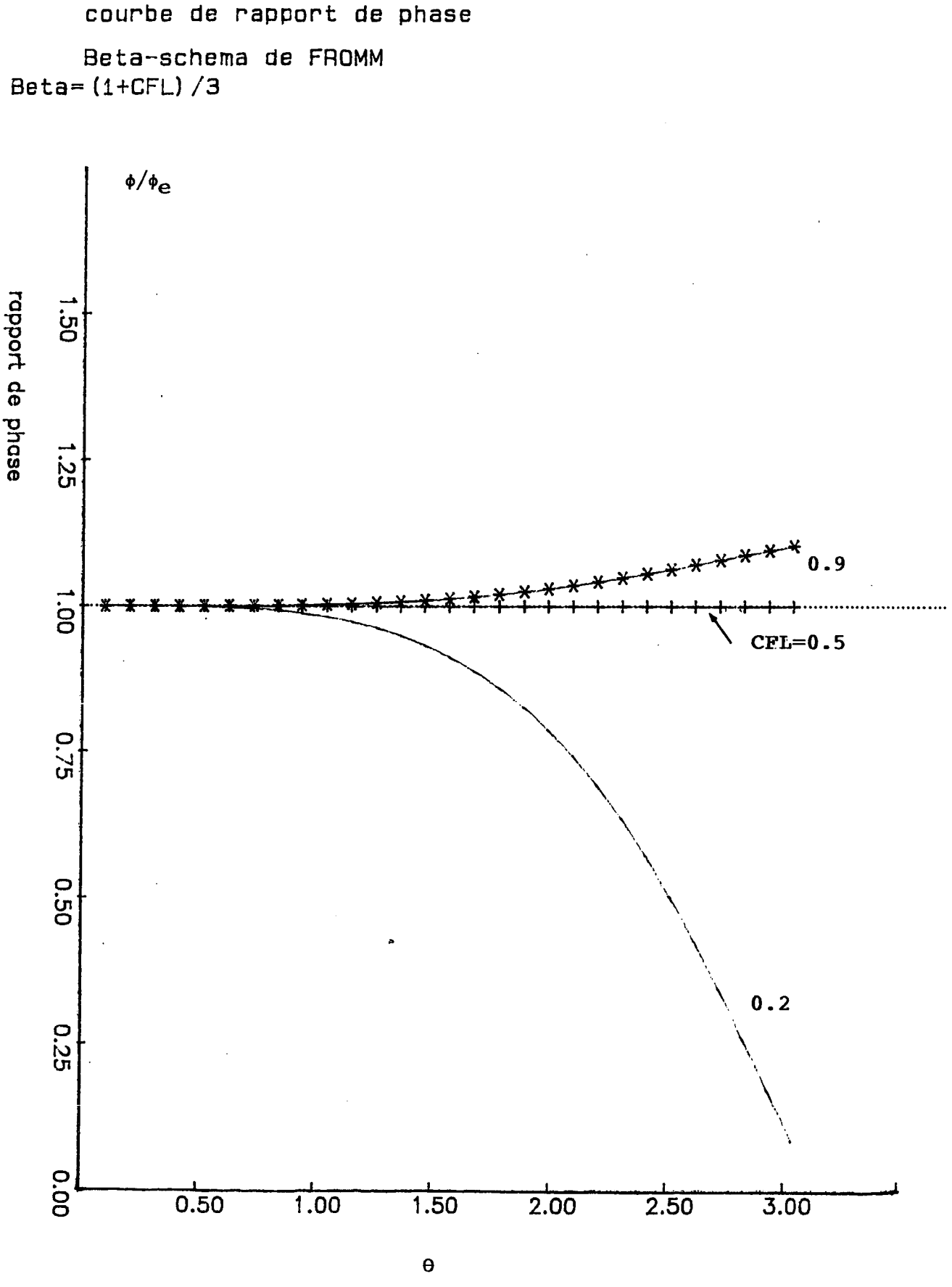

Figure 3. Phase Error (a) Fromm's scheme

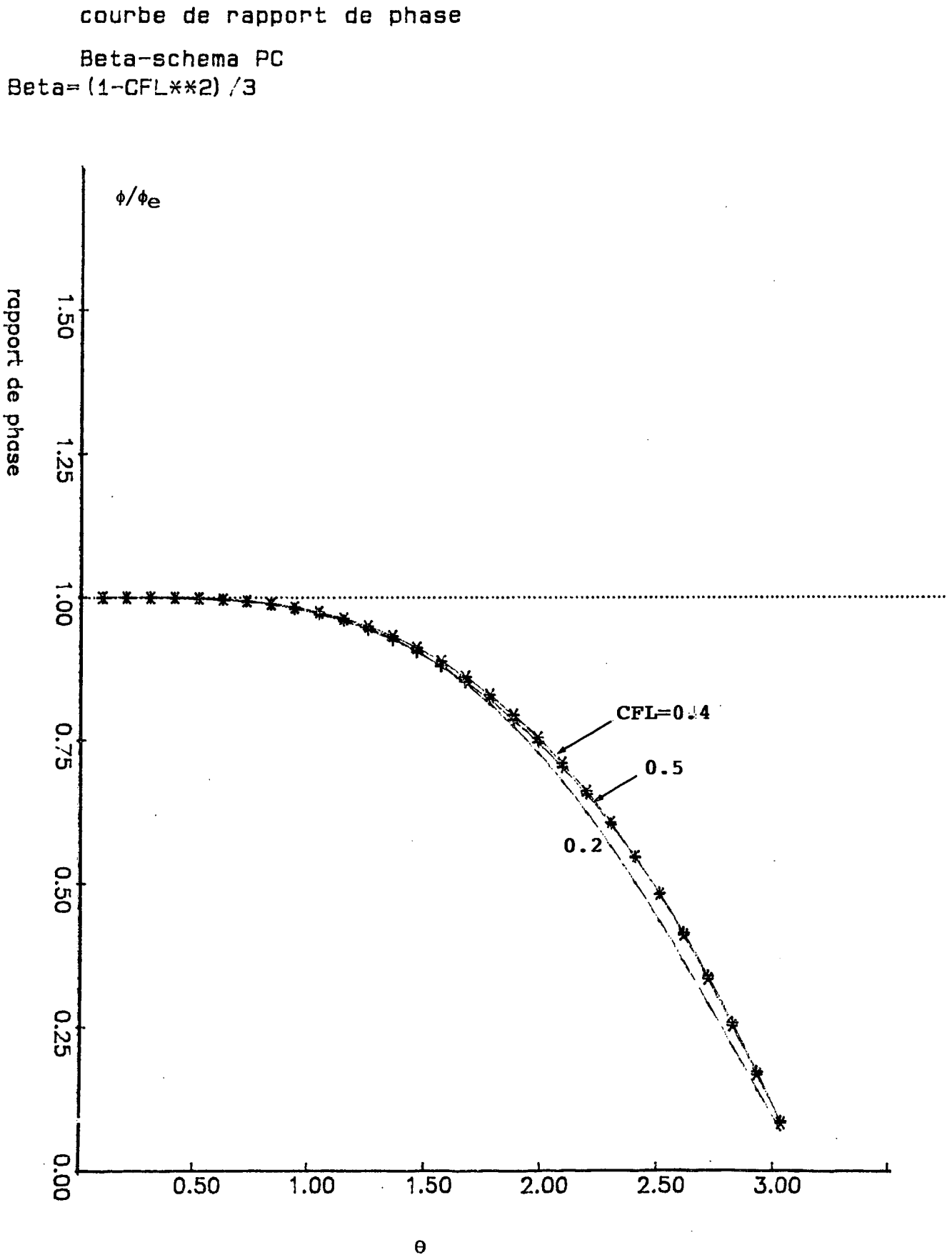

Figure 3. Cont'd (b) Predictor-Corrector scheme

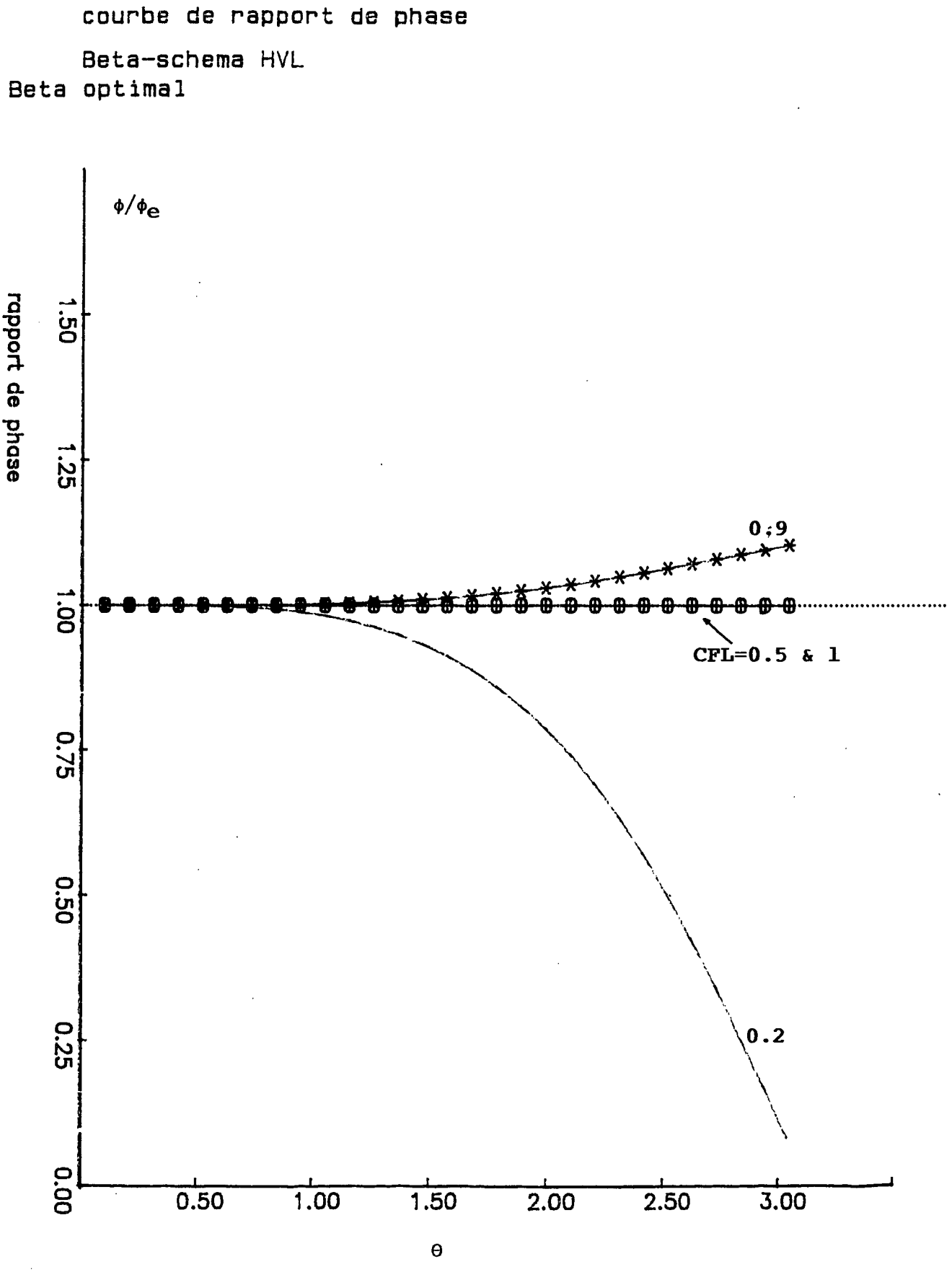

Figure 3. Cont'd (c) HVL scheme

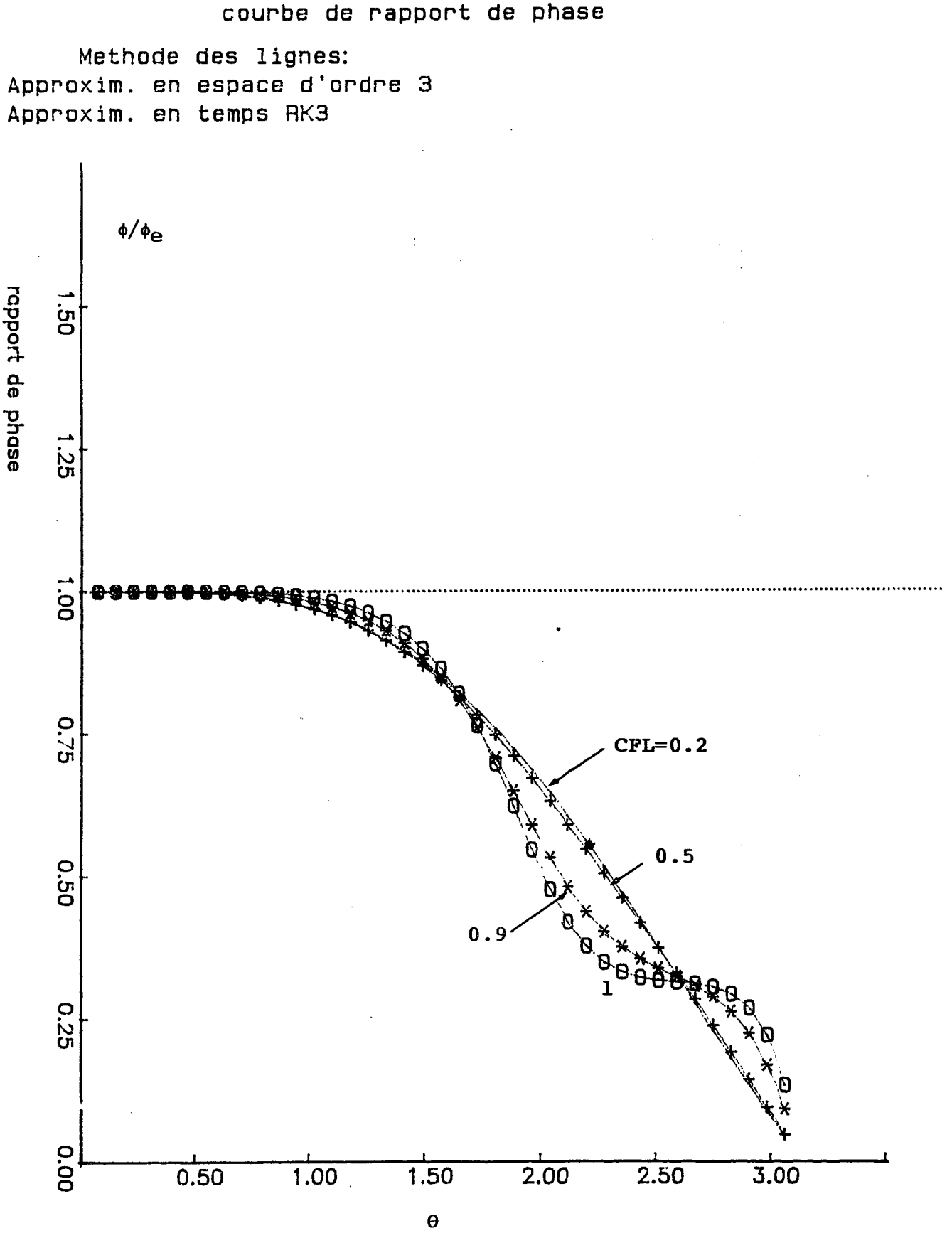

Figure 3. Concluded (d) RK3

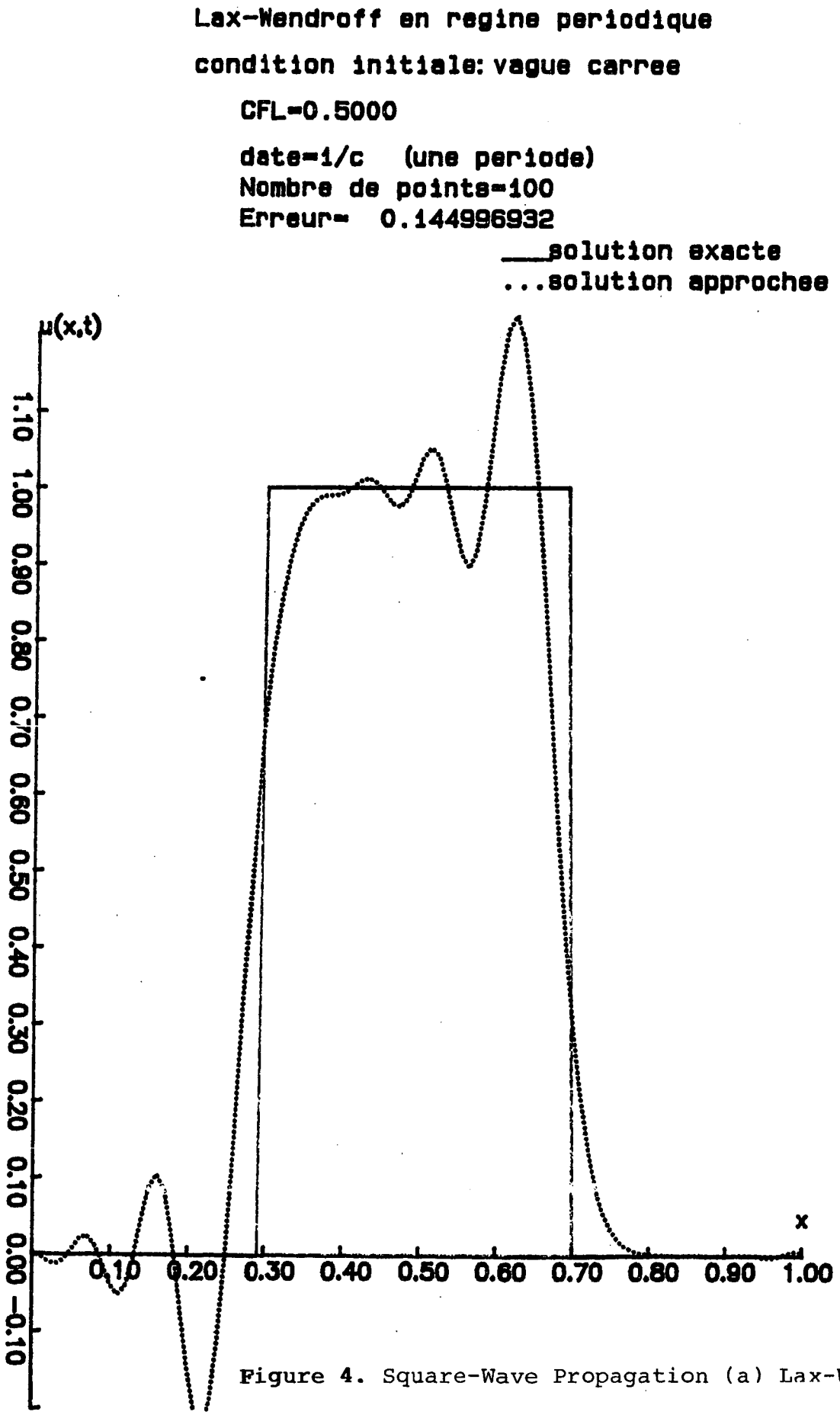

Figure 4. Square-Wave Propagation (a) Lax-Wendroff

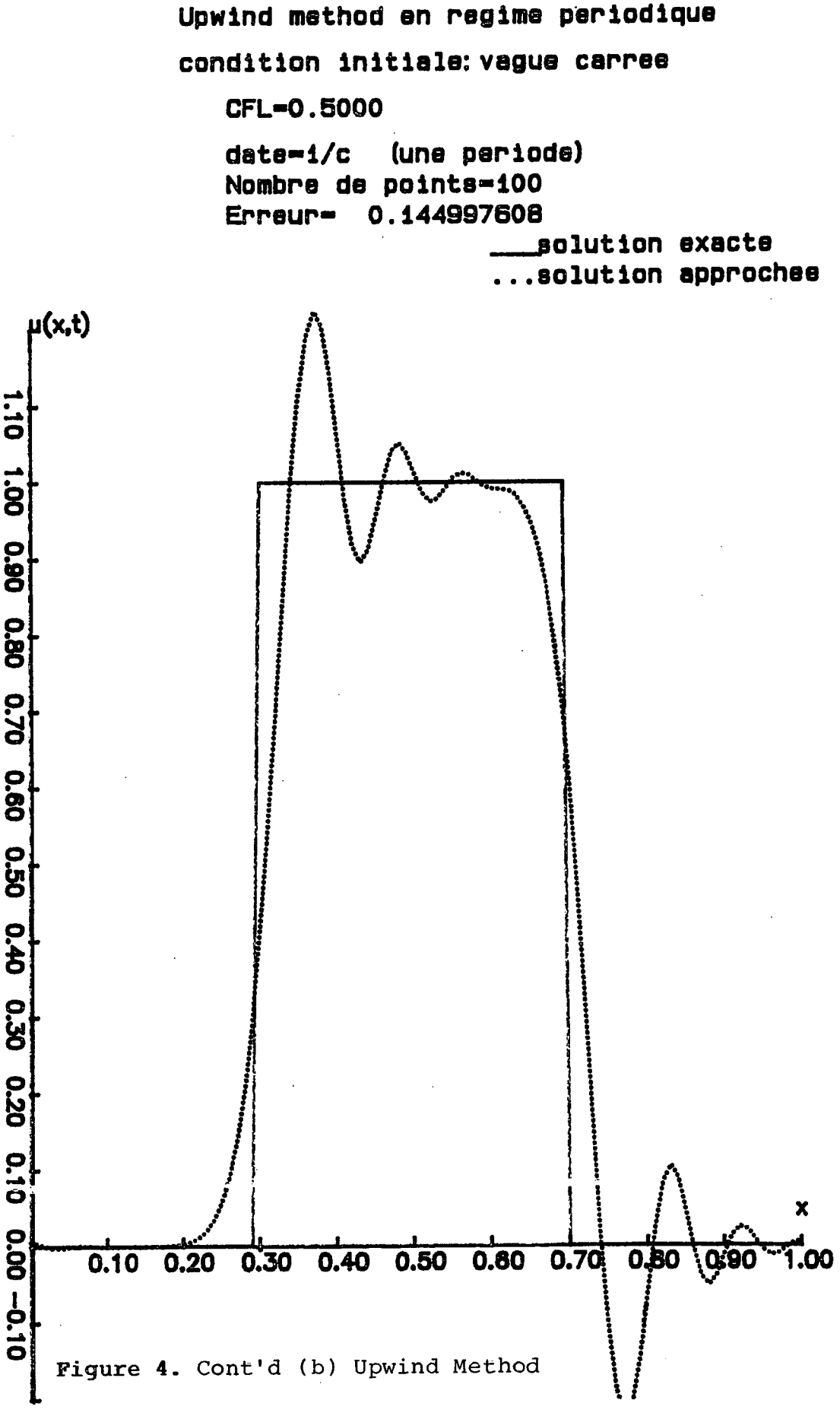

Figure 4. Cont'd (b) Upwind Method

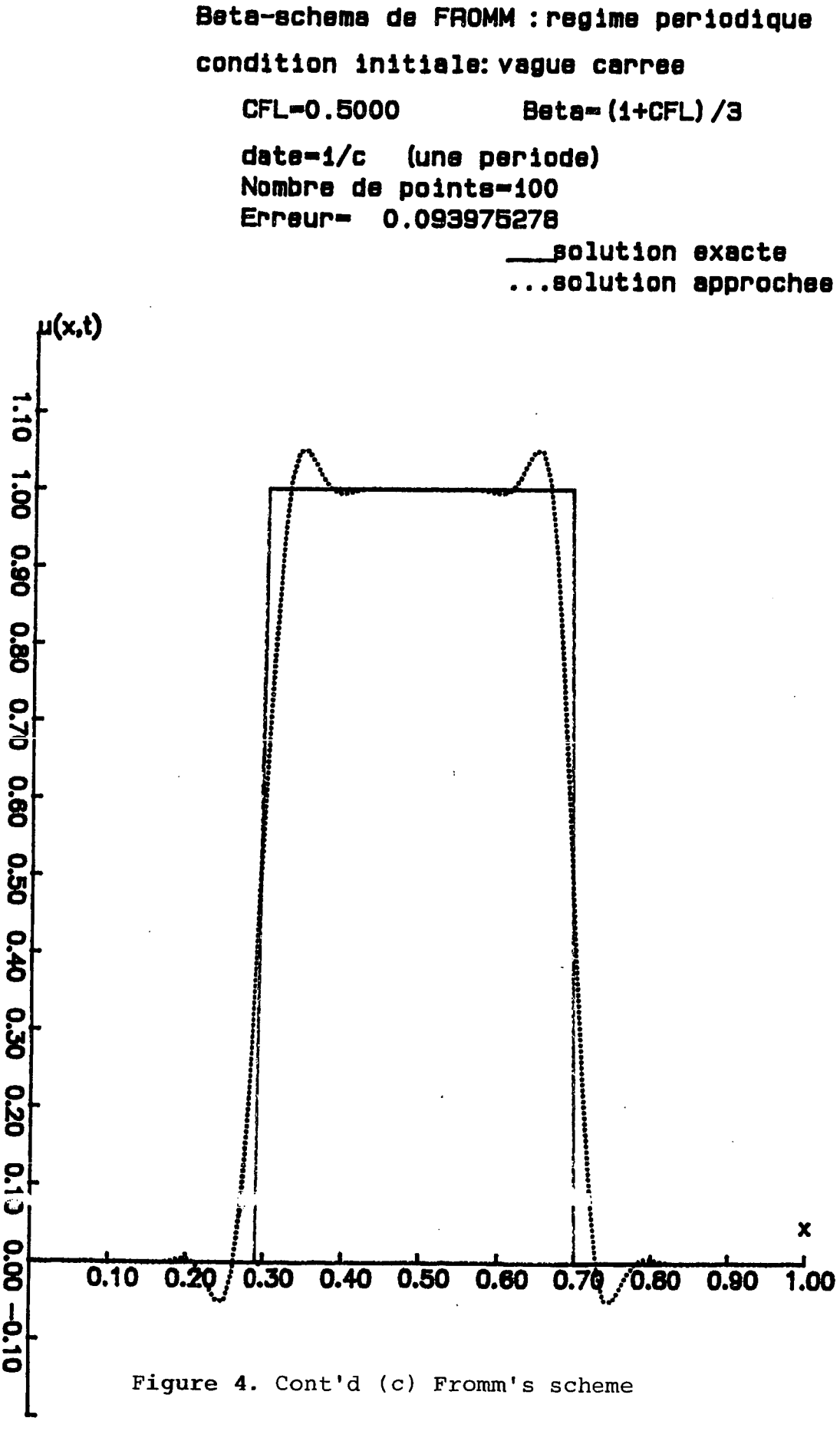

Figure 4. Cont'd (c) Fromm's scheme

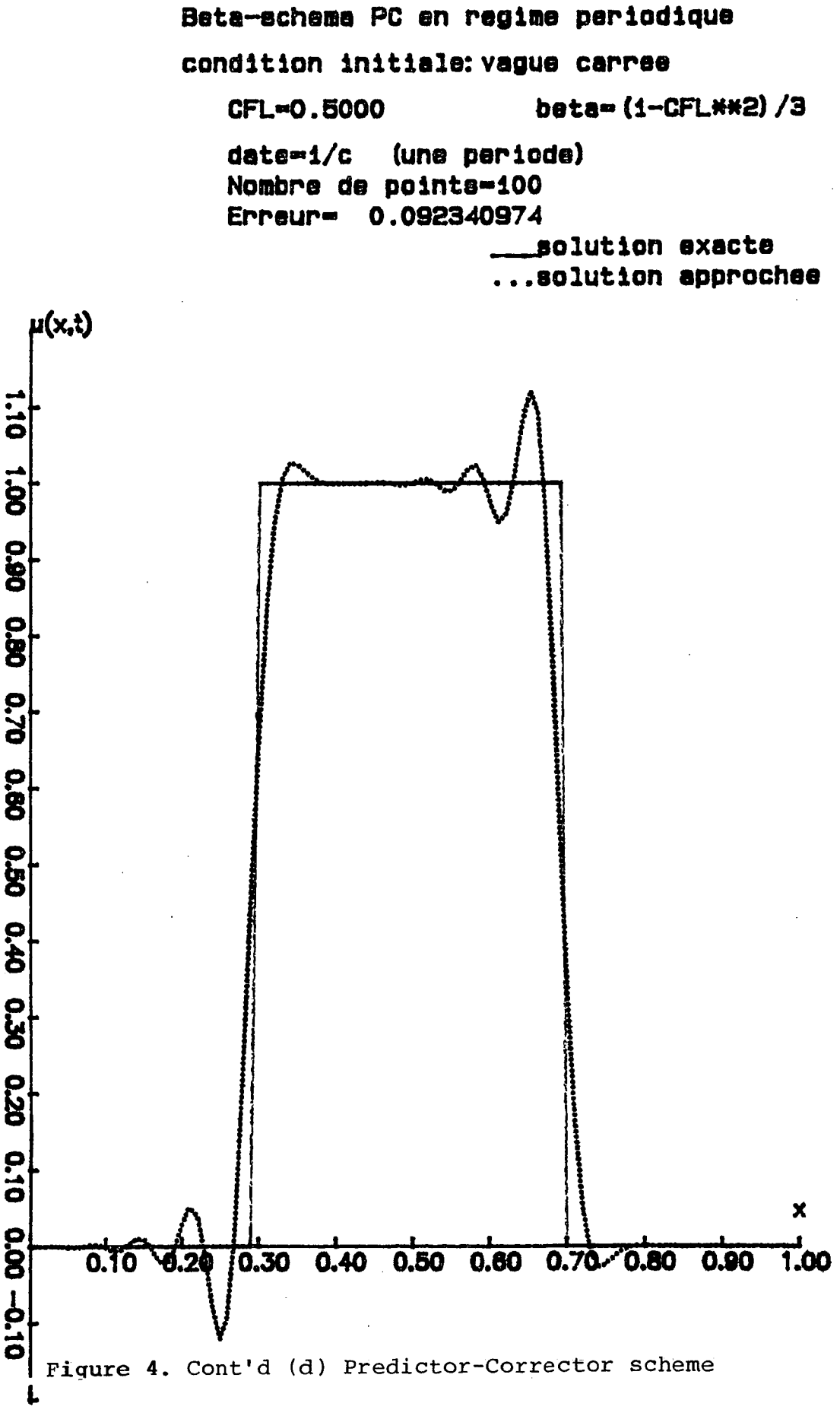

Figure 4. Cont'd (d) Predictor-Corrector scheme

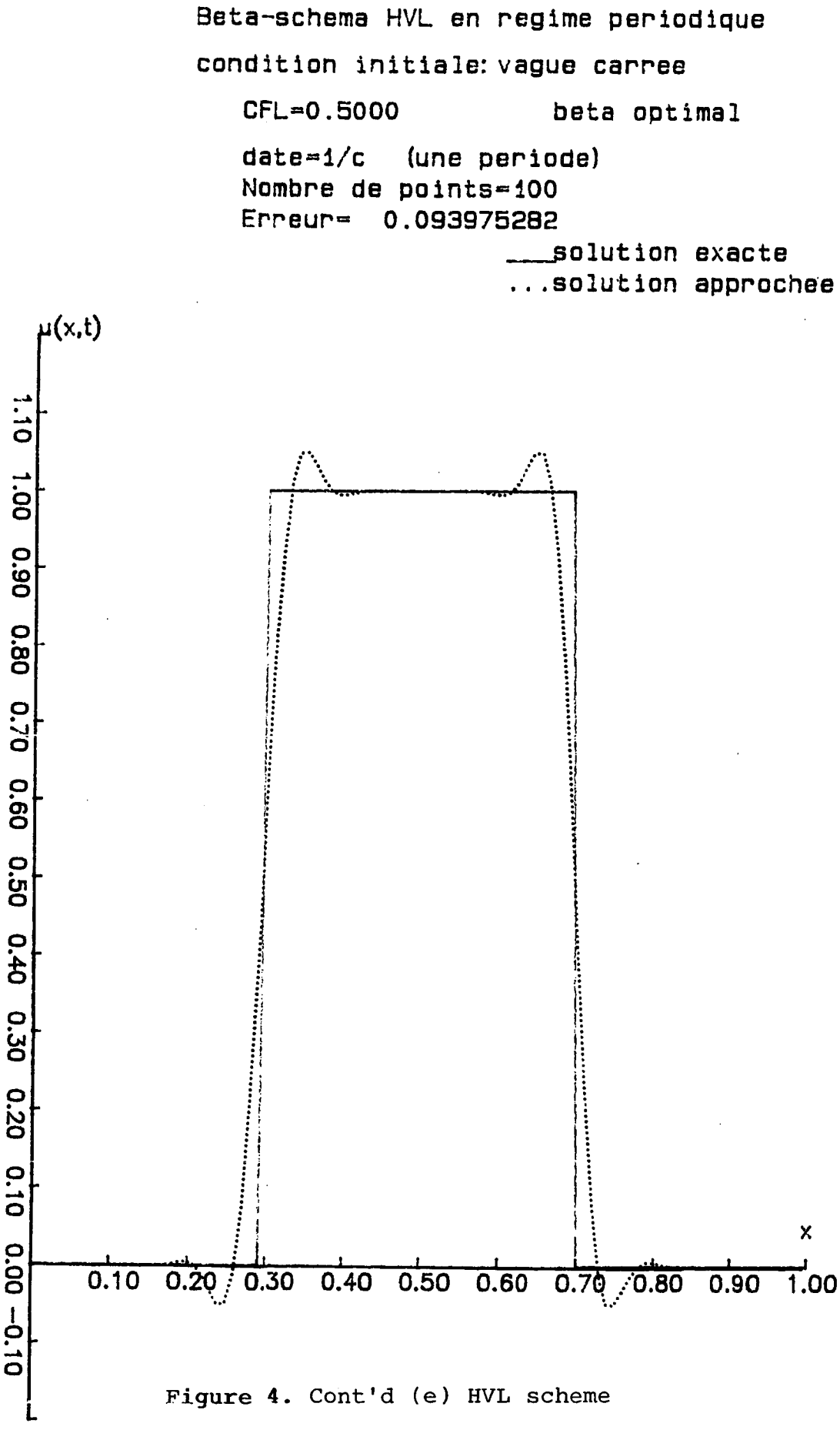

Figure 4. Cont'd (e) HVL scheme

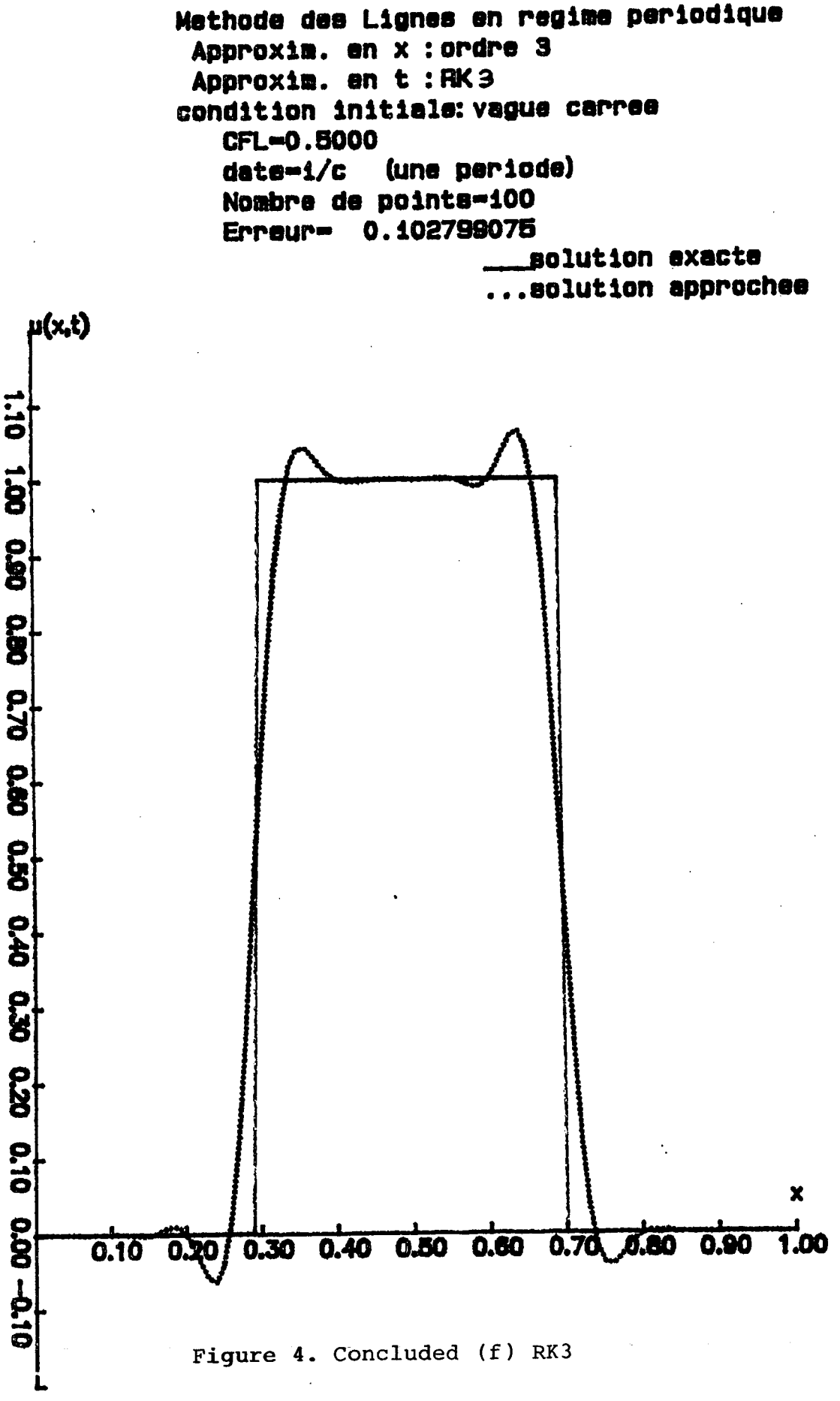

Figure 4. Concluded (f) RK3

courbe d'amplification
BETA-SCHEMA HVL 2D:
Schema demi-decentre

CFL= 0.5000

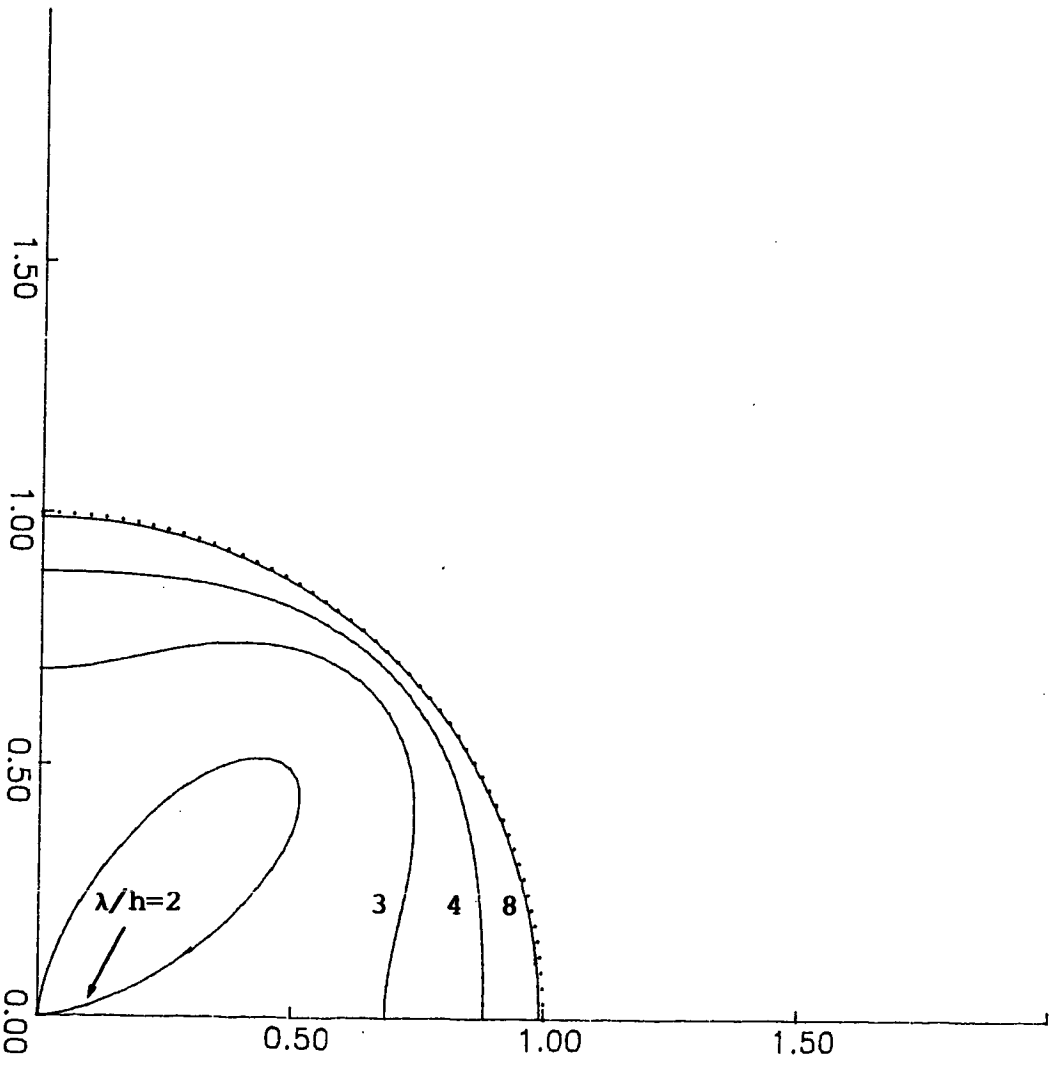

Figure 5. Dissipation Error (a) HVL

courbe d'amplification
Methode des lignes 2D:
Approxim. en espace d'ordre 3
Approxim. en temps RK3
CFL= 0.5000

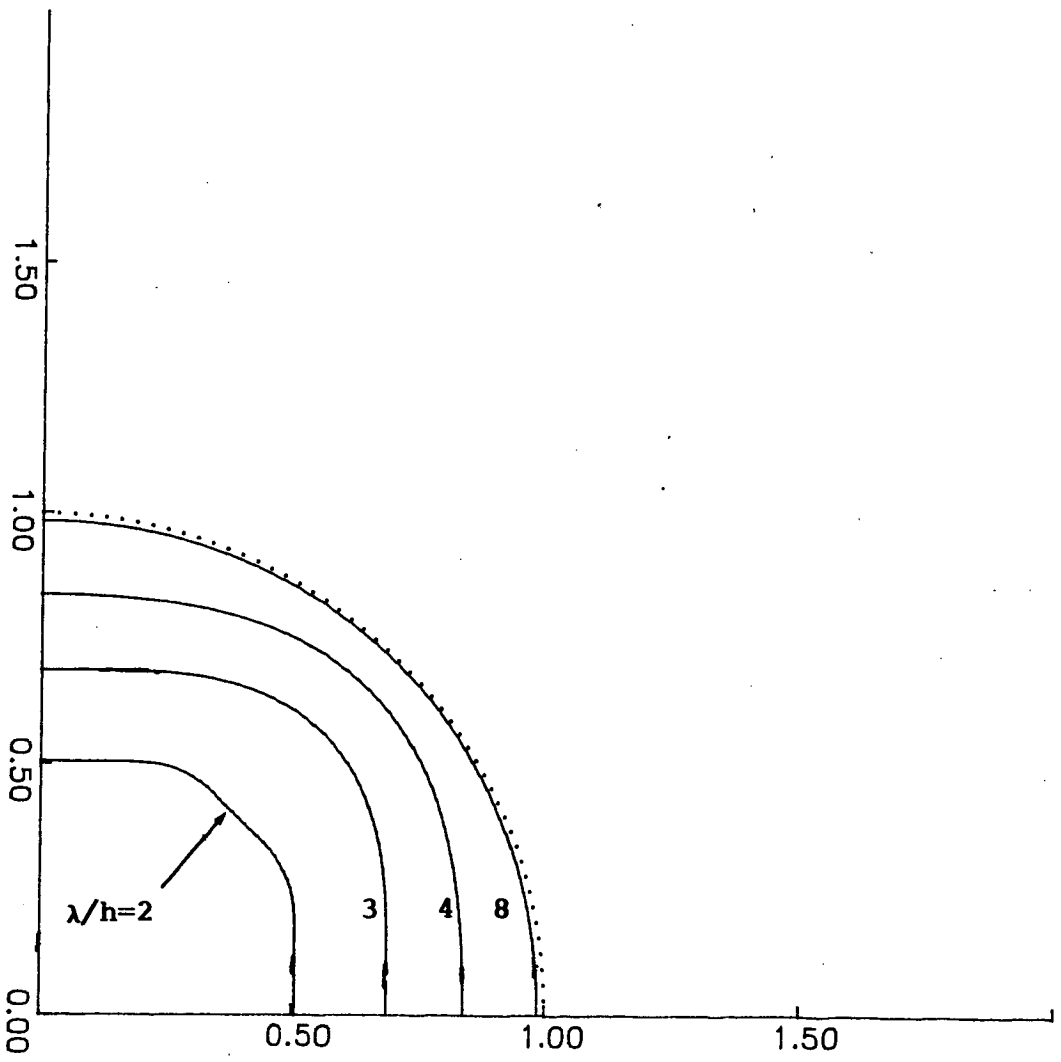

Polar representation of |g|

Figure 5. Concluded (b) RK3

courbe de rapport de phase
BETA-SCHEMA HVL 2D:
Schema demi-decentre

CFL= 0.5000

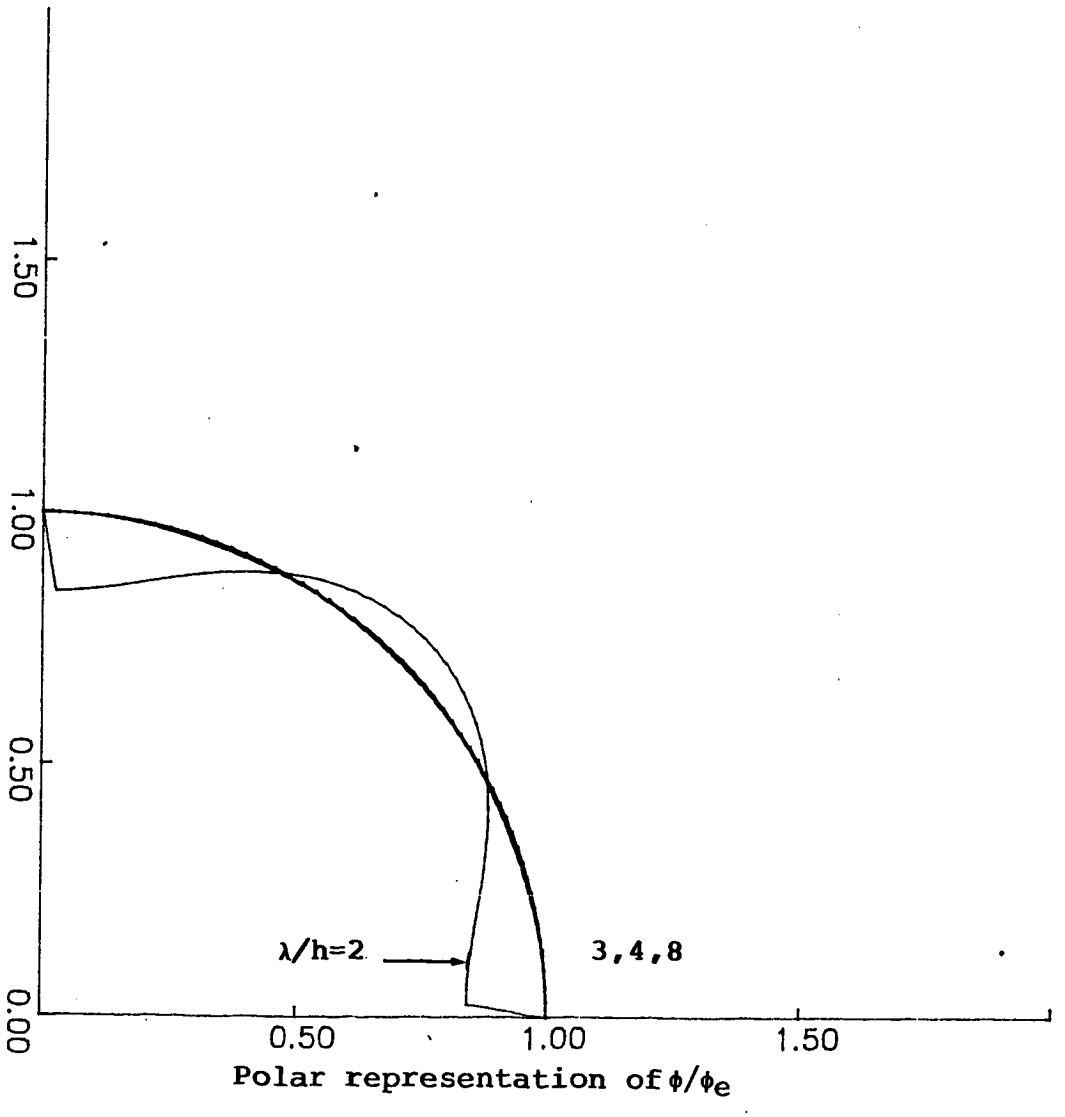

Figure 6. Phase Error (a) HVL

courbe de rapport de phase
Methode des lignes 2D:
Approxim. en espace d'ordre 3
Approxim. en temps RK3
CFL= 0.5000

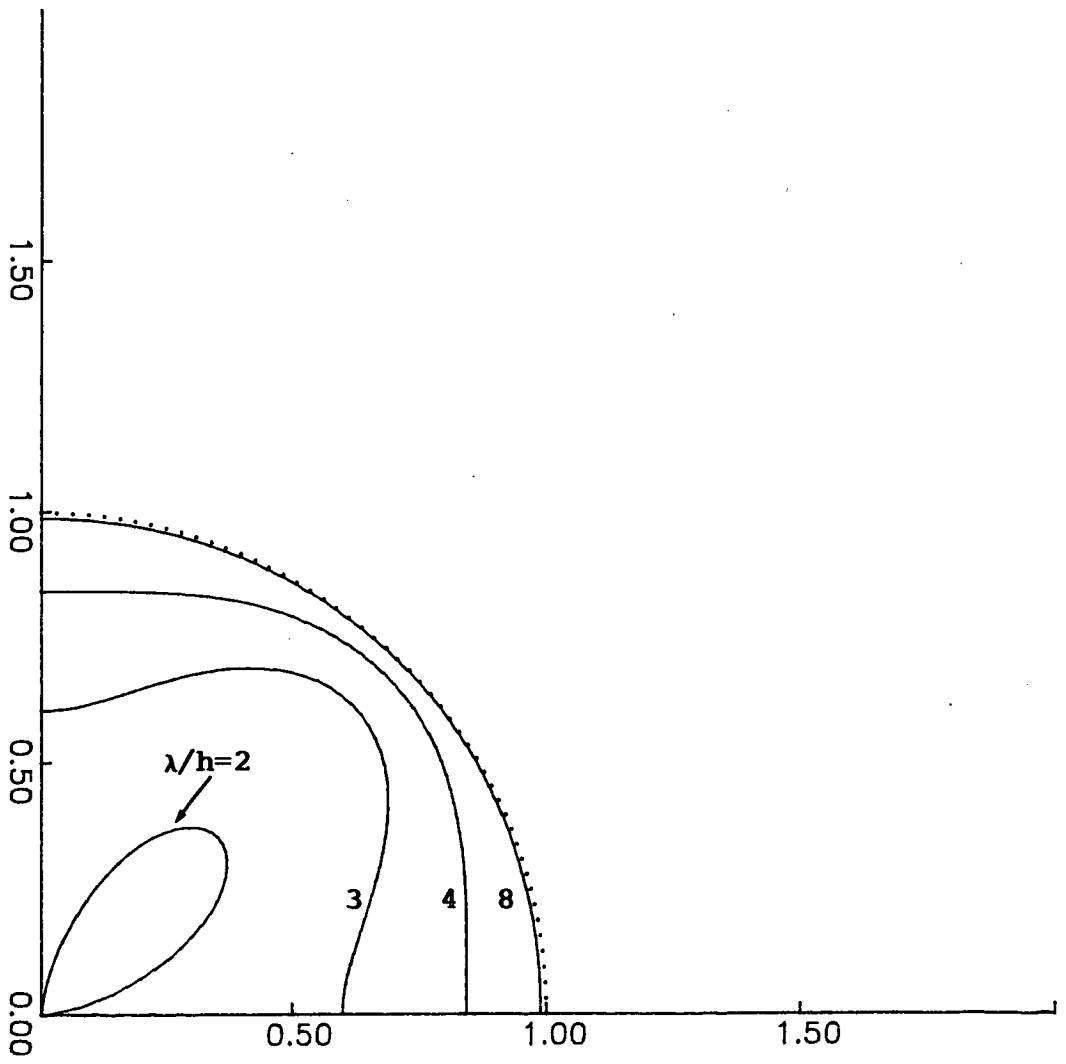

Polar representation of ϕ/ϕ_e

Figure 6. Concluded (b) RK3

HANCOCK VAN LEER
Schema 1/2decentre

Tache tournante non conique
iteration 200
Nombre de points= 961
maximum = 0.56868794 minimum = -0.00779866
Erreur= 0.06294202

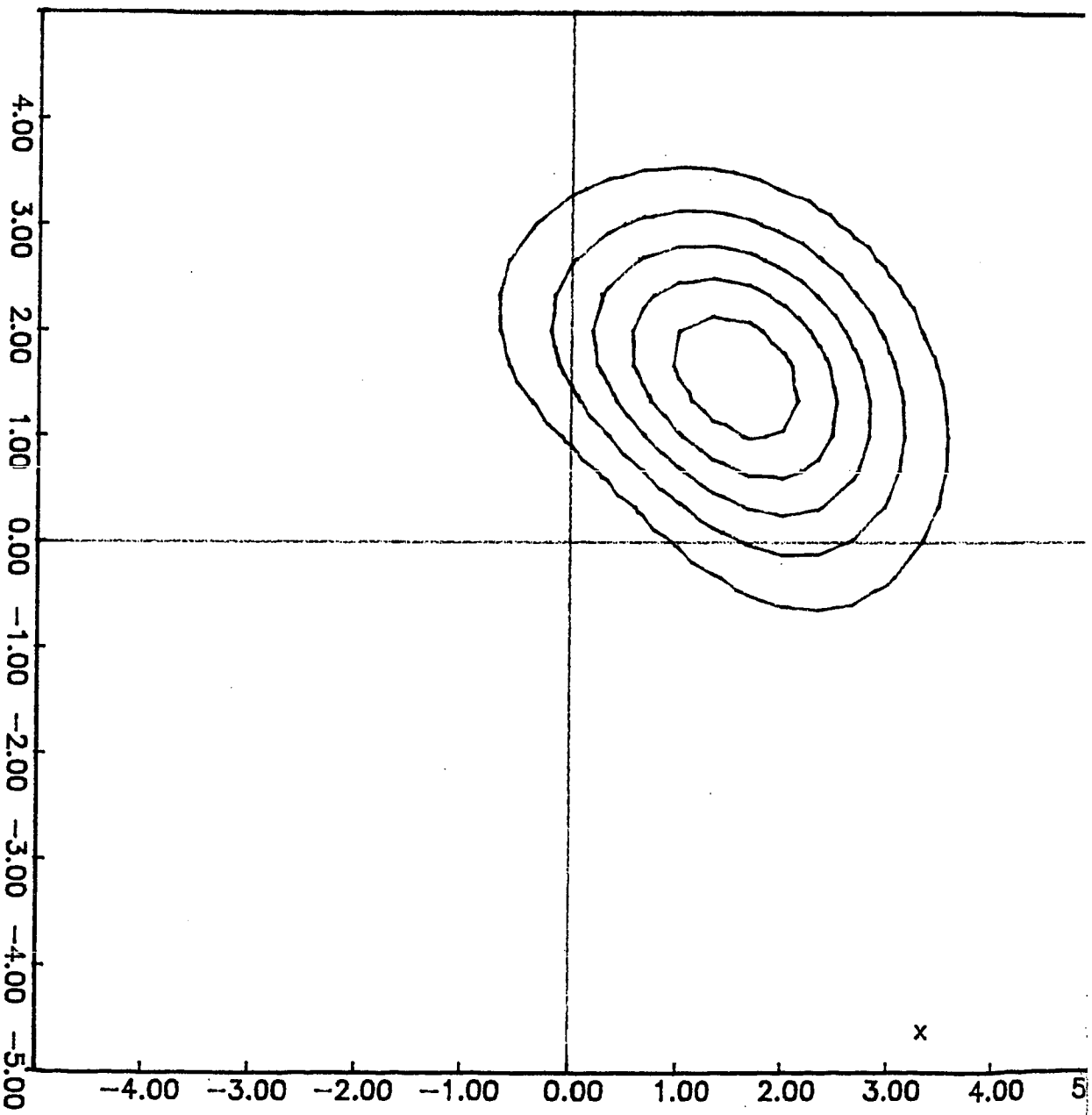

Figure 7. Problem (P1) (a) HVL

Methode des Lignes en 2-D
Approxim. en x et y: ordre 3
Approxim. en t : RK3
Tache tournante non conique
iteration 200
Nombre de points= 961
maximum = 0.83771748 minimum = -0.02352978
Erreur= 0.02445482

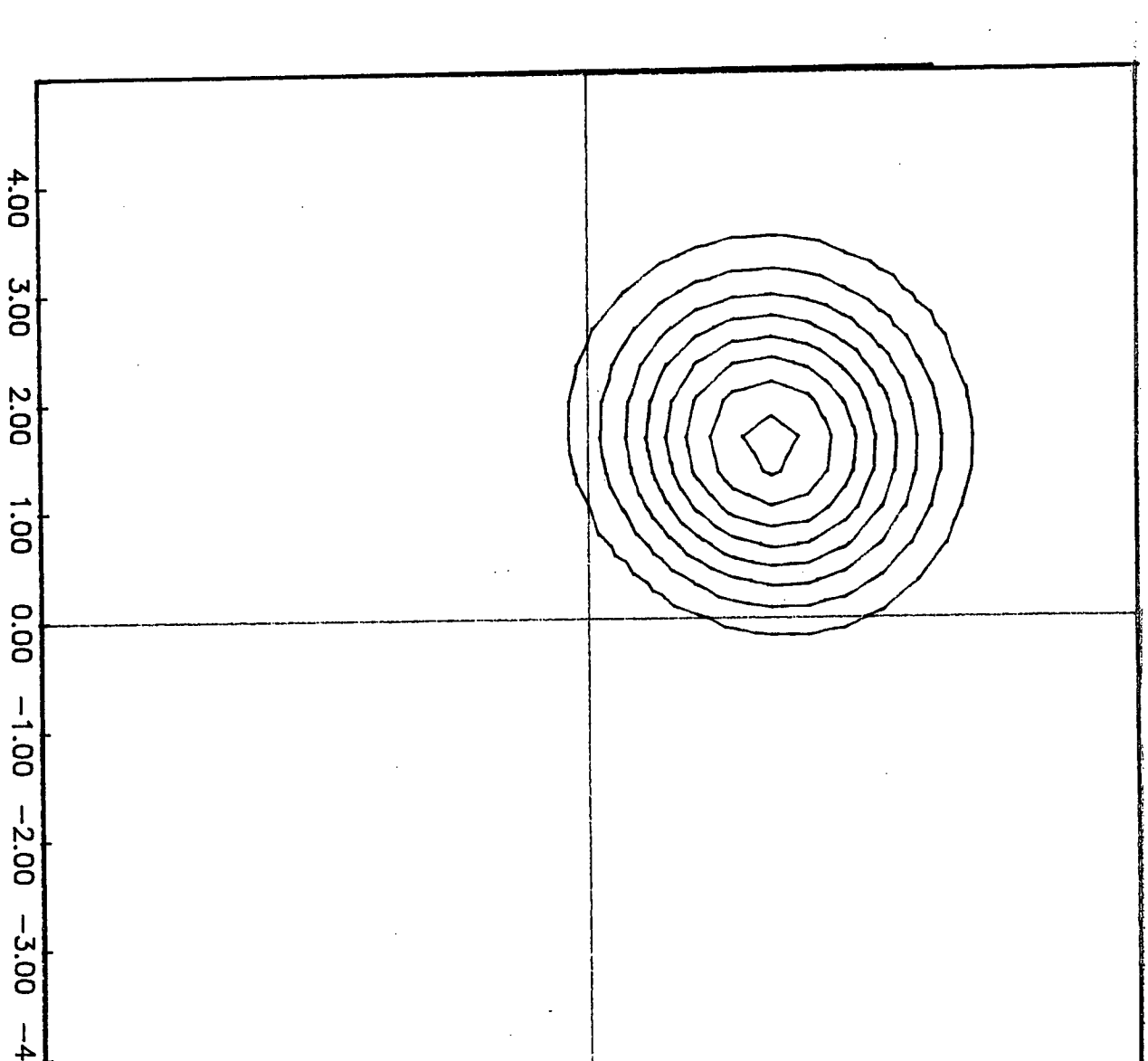

Figure 7. Cont'd (b) RK3

HANCOCK VAN LEER
Schema 1/2decentre

Tache tournante conique
iteration 200
Nombre de points= 961
maximum = 0.52949927 minimum = -0.01007768
Erreur= 0.05782345

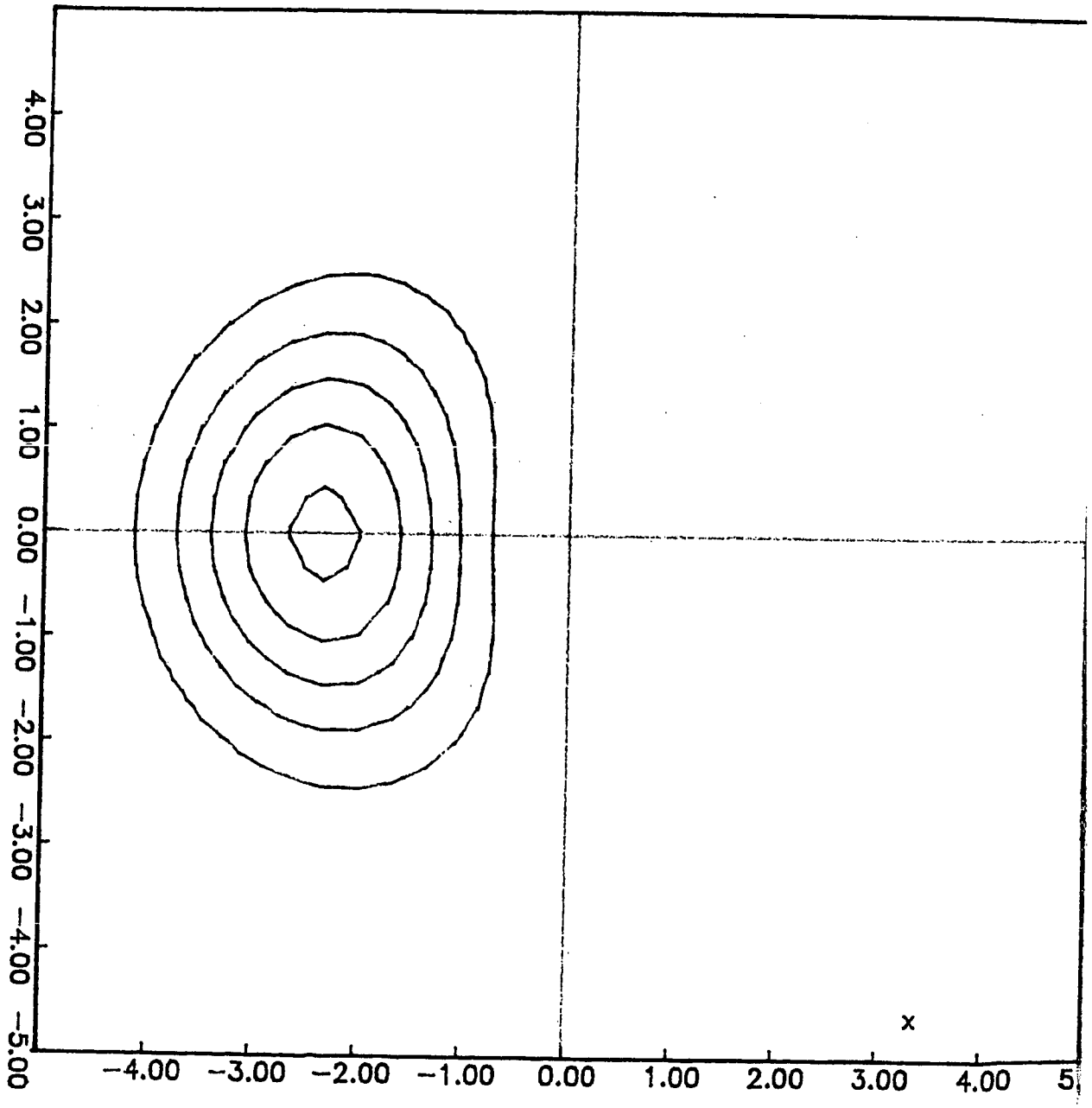

Figure 8. Problem (P2) (a) HVL

Methode des Lignes en 2-D
Approxim. en x et y: ordre 3
Approxim. en t : RK3
Tache tournante conique
iteration 200
Nombre de points= 961
maximum = 0.75764012 minimum = -0.01867521
Erreur= 0.0200462

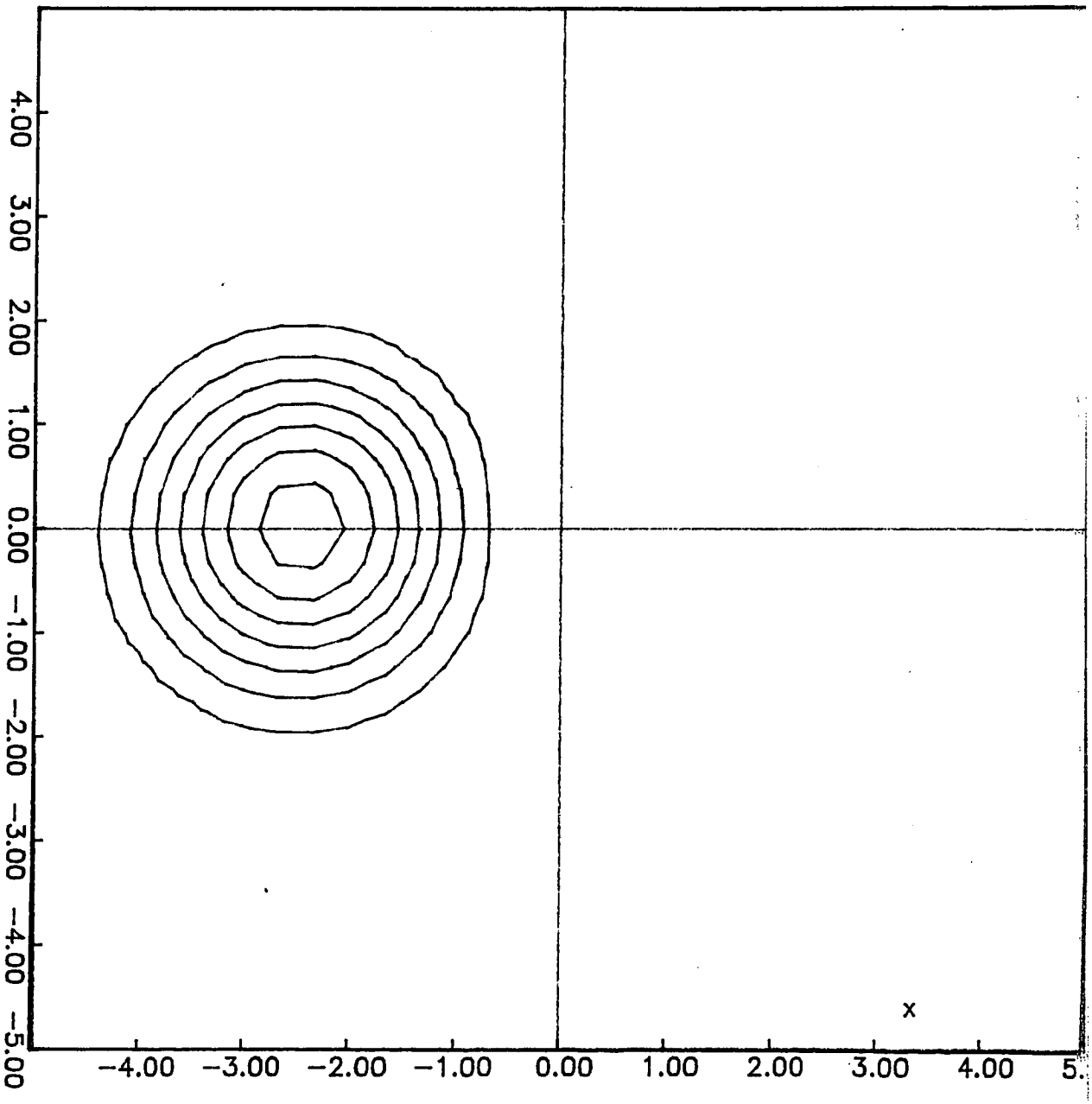

Figure 8. Cont'd (b) RK3

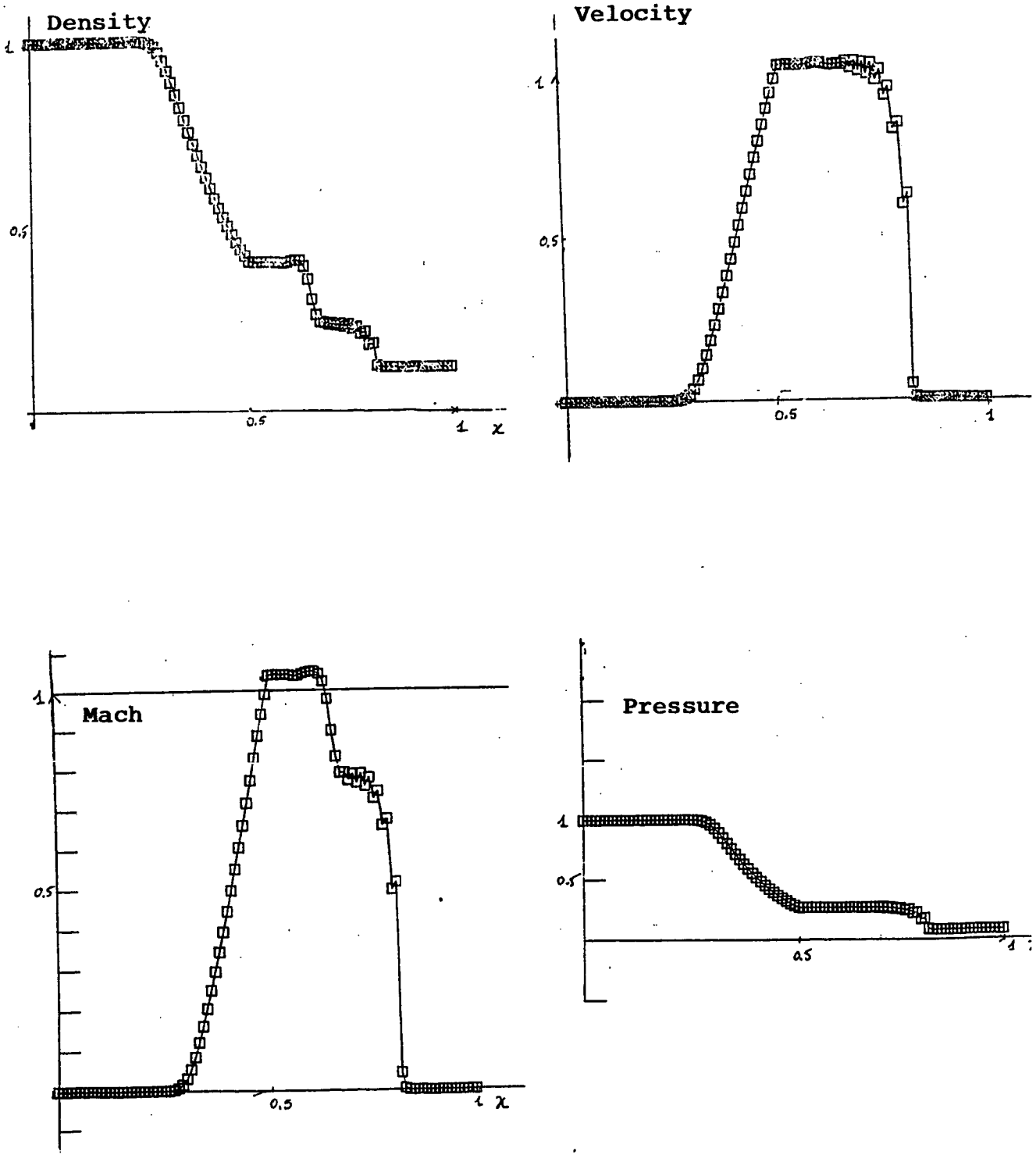

Figure 9. Shock-Tube Problem. HVL (a) β =1/2

(CFL=0.8)

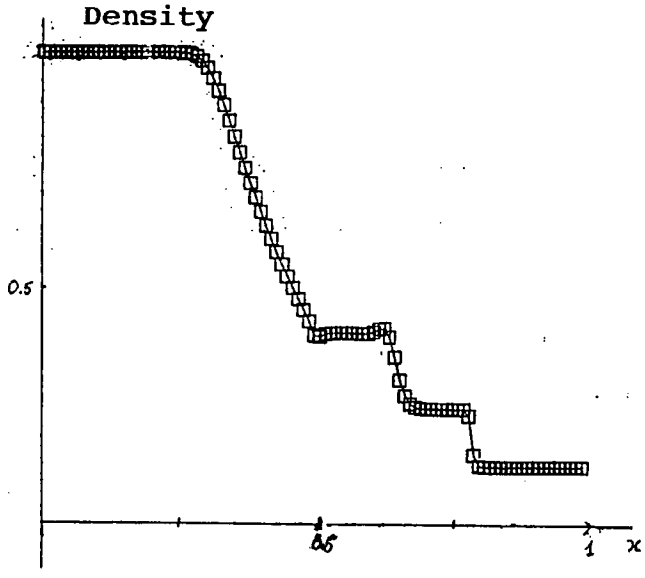

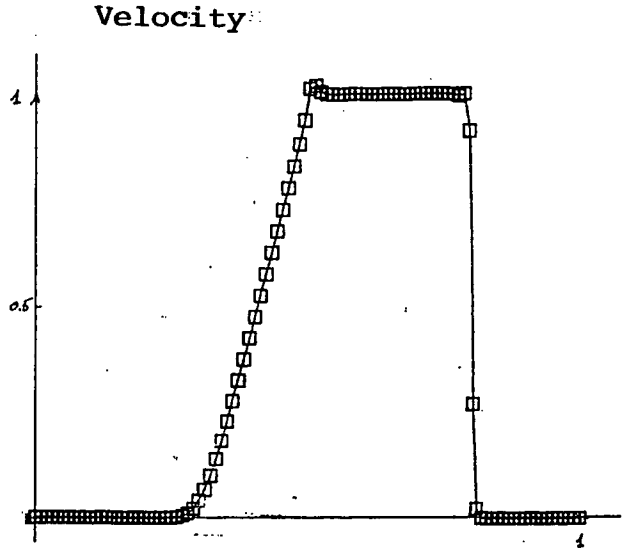

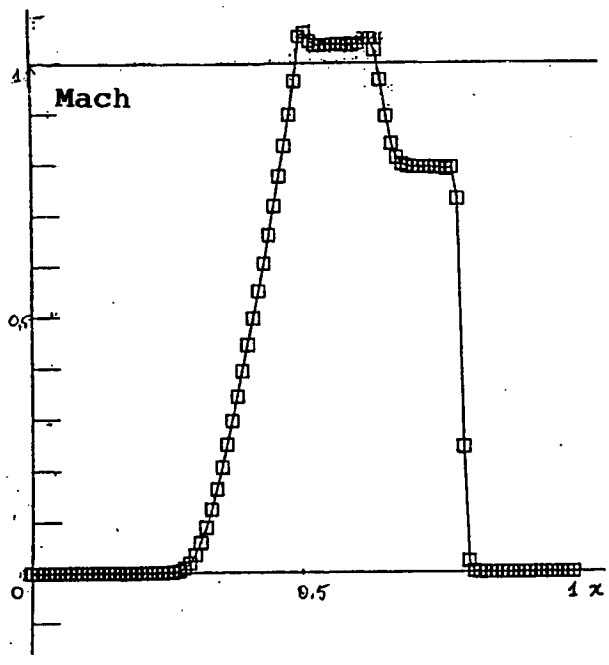

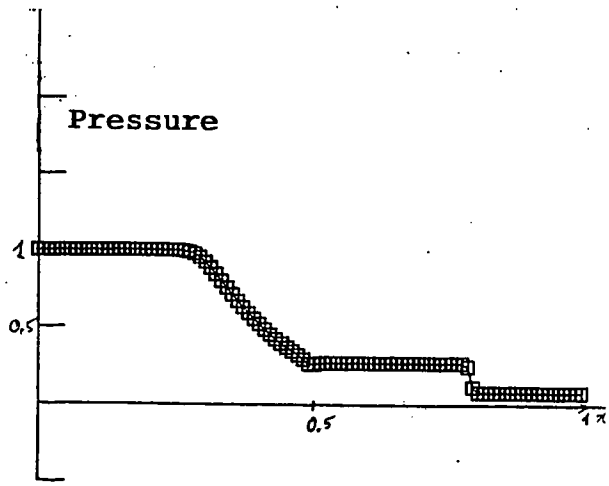

Figure 9. Cont'd (b) $\beta = 1/3$.

(CFL=0.8)

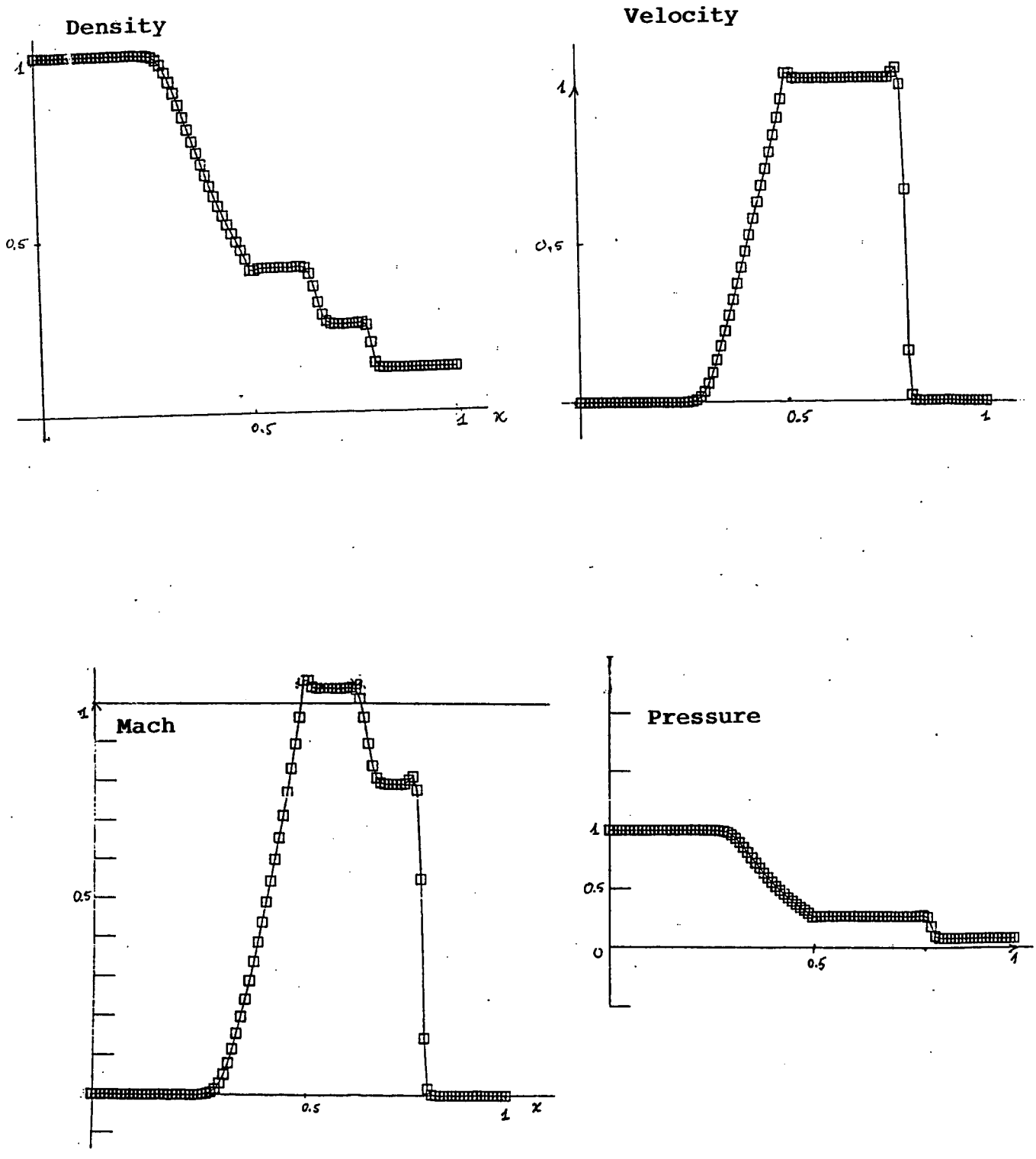

Figure 10. Shock-Tube Problem. RK3 - $\beta = 1/3$ (CFL=0.8)

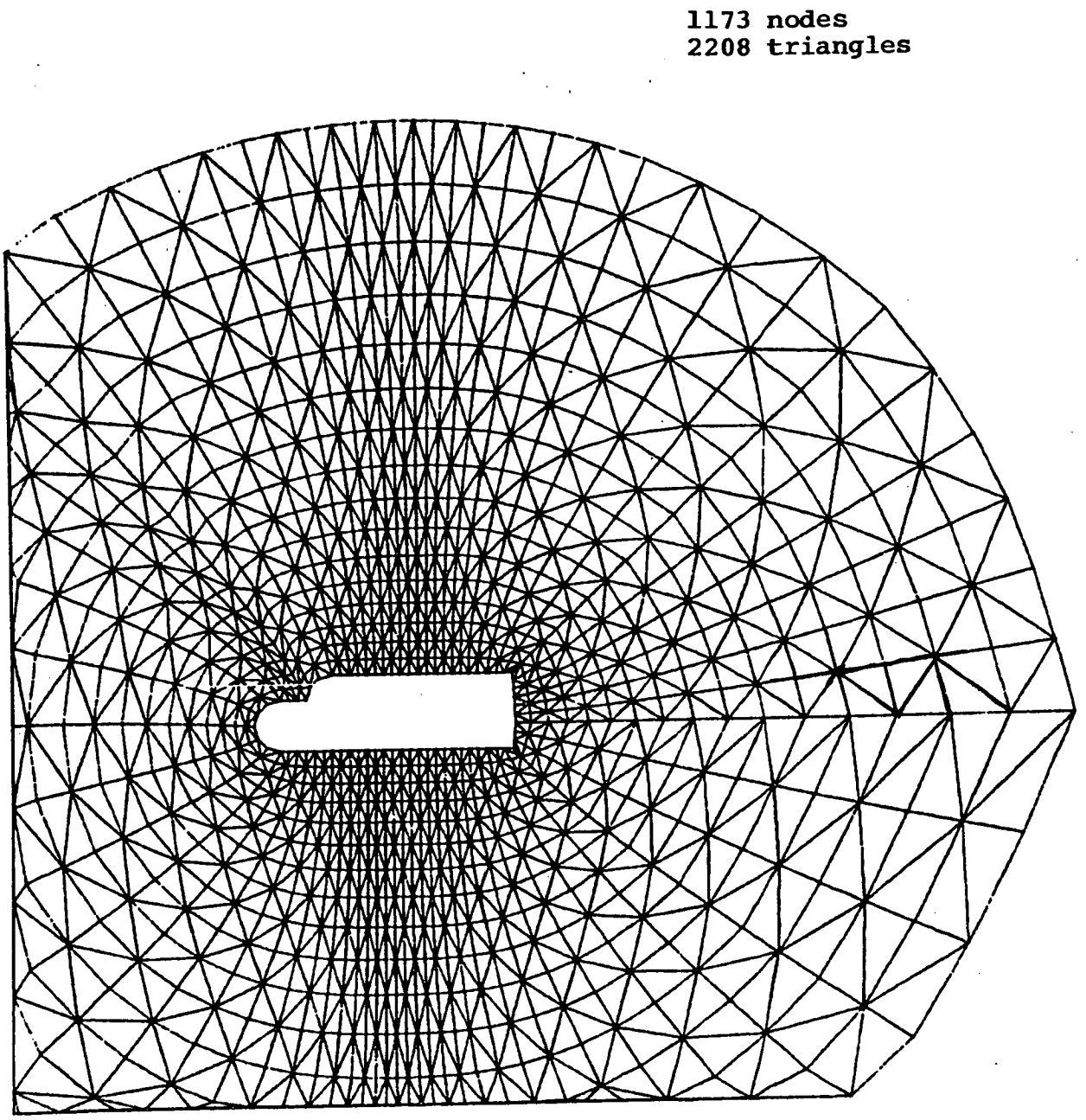

Figure 11. Finite-Element Mesh for 2-D Euler computation

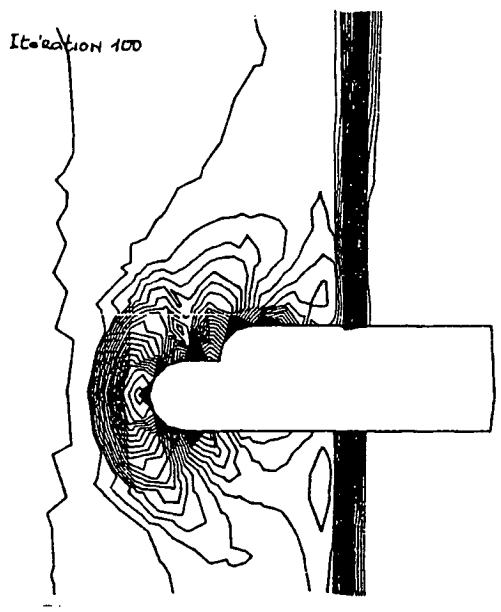

a

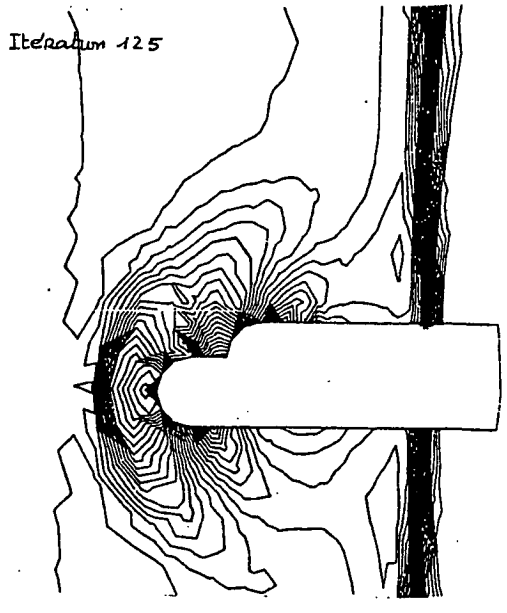

b

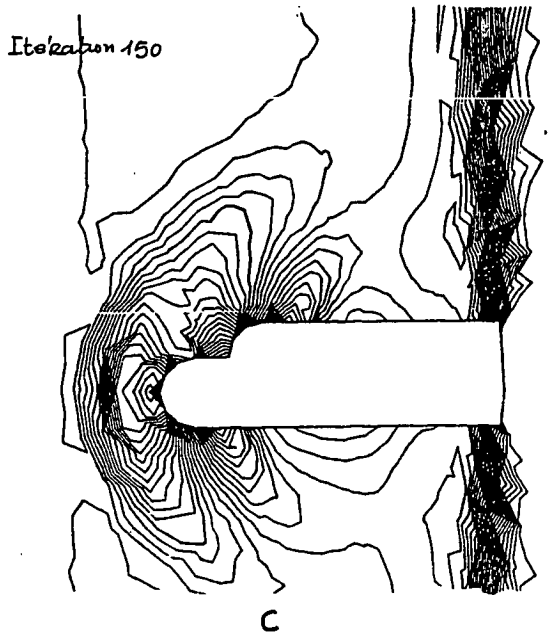

c

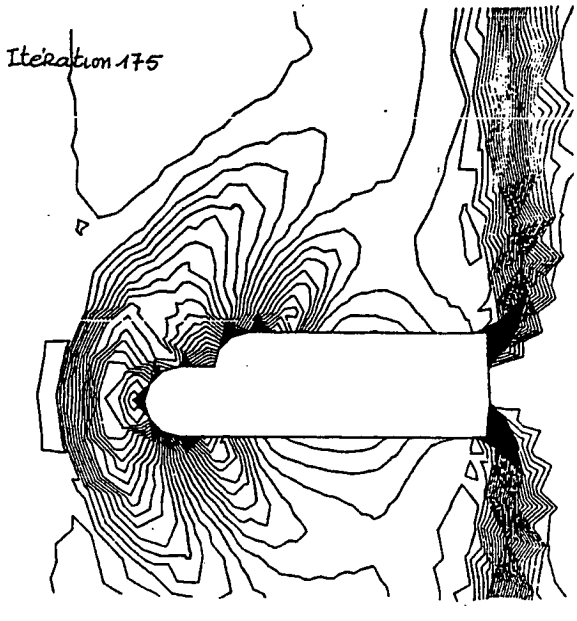

d

Imprimé en France
par
l'Institut National de Recherche en Informatique et en Automatique